On the observed ecohydrologic dynamics of a semiarid basin with aspect-delimited ecosystems

Hugo A. Gutiérrez-Jurado,[1,2] Enrique R. Vivoni,[3] Colin Cikoski,[2] J. Bruce J. Harrison,[2] Rafael L. Bras,[4] and Erkan Istanbulluoglu[5]

Received 2 July 2013; revised 12 November 2013; accepted 18 November 2013; published 11 December 2013.

[1] In semiarid complex terrain, the combination of elevation and aspect promotes variations in the water and energy balance, resulting in slopes with distinct ecologic and hydrologic properties. Quantifying the differential energy and water dynamics of opposing slopes can provide essential information on the potential effects of climate variability on landscapes. In this study, we use observations from a network of hydrologic sensors deployed on the slopes of a semiarid catchment in central New Mexico, USA, to quantify the ecohydrologic dynamics of two coexisting and contrasting ecosystems: a juniper (*Juniperus monosperma*) savanna on a north facing slope (NFS) and a creosote (*Larrea tridentata*) shrubland on a south facing slope (SFS). Our analyses show that: (1) energy loads exert a first-order control on the dynamics of evapotranspiration and soil moisture residence times in the catchment, with vegetation imposing a second-order control at the onset of the growing season; (2) soils exhibit a characteristic progression of moisture and temperature along the slope-aspect continuum that is preserved throughout the year, going from a wetter and cooler NFS to a drier and warmer SFS; (3) there are remarkable differences in the runoff dynamics among the catchment slopes, with a smaller precipitation threshold triggering larger SFS runoff amounts than at its NFS counterpart; and (4) seasonal water balances of the NFS and SFS follow opposite trajectories in the year and point to distinct soil water pools for evapotranspiration demands. The results of this study have important implications for understanding landscape changes in areas of complex topography under current and future climate variability.

Citation: Gutiérrez-Jurado, H. A., E. R. Vivoni, C. Cikoski, J. B. J. Harrison, R. L. Bras, and E. Istanbulluoglu (2013), On the observed ecohydrologic dynamics of a semiarid basin with aspect-delimited ecosystems, *Water Resour. Res.*, *49*, 8263–8284, doi:10.1002/2013WR014364.

1. Introduction

[2] Understanding the coupling of terrain, vegetation, and hydrology can reveal important constraints on the distribution and adaptability of plants to a varying range of environmental conditions, and at the same time help in clarifying the role of plants in the water balance of catchments [*Brooks and Vivoni*, 2008; *Vivoni et al.*, 2010]. The role of terrain aspect on vegetation patterns has received attention as a proxy for variable environmental conditions and their differing responses to climate variability [e.g., *Broxton et al.*, 2009]. For example, *Armesto and Martínez* [1978] showed that differences in vegetation composition responded to a nonlinear moisture trend following variations in aspect, while *Wang et al*. [2011] showed that vegetation species and aspect significantly influence the water budget in the soil-vegetation-atmospheric continuum. Yet, these complex terrain-vegetation-hydrologic interactions are poorly understood and have not been systematically quantified [*Tromp-van Meerveld and McDonnell*, 2006]. This is partly owing to the difficulty of capturing, either by direct observation or modeling efforts, the large number of nonlinear processes interacting at various temporal and spatial scales within areas of complex terrain and vegetation assemblages [*Ivanov et al*., 2008a; *Vivoni*, 2012]. Nonetheless, the systematic investigation of feedbacks and interactions of vegetation and water fluxes in semiarid catchments with complex topography can improve our understanding and predictive capabilities of potential hydrologic and ecologic regime shifts [*Newman et al*., 2006], especially in areas with a fragile equilibrium or dynamic ecotones.

[1]National Centre for Groundwater Research and Training, School of the Environment, Flinders University, Adelaide, South Australia, Australia.
[2]Department of Earth and Environmental Science, New Mexico Institute of Mining and Technology, Socorro, New Mexico, USA.
[3]School of Earth and Space Exploration, School of Sustainable Engineering and the Built Environment, Arizona State University, Tempe, Arizona, USA.
[4]School of Civil and Environmental Engineering, School of Earth and Atmospheric Sciences, Georgia Institute of Technology, Atlanta, Georgia, USA.
[5]Department of Civil and Environmental Engineering, University of Washington, Seattle, Washington, USA.

Corresponding author: H. A. Gutiérrez-Jurado, National Centre for Groundwater Research and Training, School of the Environment, Flinders University, GPO Box 2100, Adelaide, SA 5001, Australia. (hugo.gutierrez@flinders.edu.au)

0043-1397/13/10.1002/2013WR014364

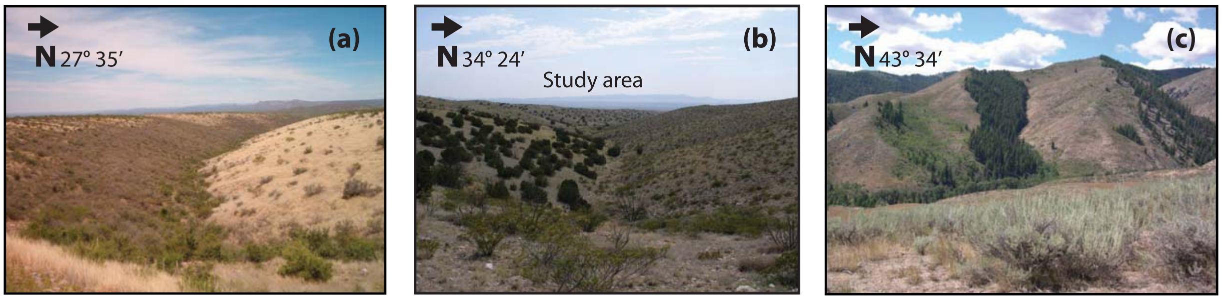

Figure 1. Semiarid basins with contrasting vegetated slopes along a latitudinal gradient in North America: (a) slopes of central Chihuahua, Mexico, with deciduous woody vegetation on the north facing slopes and grasses and shrubs on the south facing slope; (b) slopes in central New Mexico, USA, with juniper trees and grasses on the north facing slopes and shrubs and grasses on the south facing slopes; and (c) slopes near Anderson Ranch, Idaho, USA, showing conifer trees on the north facing slopes and grasses on the south facing slopes (reproduced with permission from Thayne Tuason, Central Washington Native Plants, http://www.cwnp.org/).

[3] In semiarid areas, the contrasting effects of aspect on the modification of environmental variables to which vegetation is highly sensitive give way to the emergence of coexisting ecosystems [*Mooney et al*., 1975; *Badano et al*., 2005]. These aspect-delimited ecosystems, found in very close proximity, have recognizably distinct hydrologic functioning and aridity tolerances that in normal conditions would be separated by large distances and/or significant differences in elevation [*Whittaker*, 1967; *Méndez-Barroso et al*., 2009]. In this context, performing comparative studies of aspect-delimited ecosystems in areas with complex terrain provide opportunities to examine how changes in land surface properties might impact the ecohydrologic dynamics of semiarid ecosystems [*Turnbull et al*., 2010c]. The natural arrangement of vegetation with terrain slope and aspect is a global phenomenon that is common to mid-latitude regions [*Cottle*, 1932; *Cantlon*, 1953; *Holland and Steyn*, 1975; *Mooney et al*., 1975; *Parsons and Moldenke*, 1975; *Parsons*, 1976; *Holland et al*., 1977; *Armesto and Martínez*, 1978; *Kutiel*, 1992; *Kutiel and Lavee*, 1999; *Sternberg and Shoshany*, 2001; *Desta et al*., 2004; *Badano et al*., 2005; *Gutiérrez-Jurado et al*., 2006; *Astrom et al*., 2007; *Bennie et al*., 2008b; *Chmura*, 2008; *Gallardo-Cruz et al*., 2009; *Warren*, 2010]. Figure 1 provides an example of vegetation differences between "equator-facing" and "pole-facing" slopes at three different latitudes in North America. In the cases shown, a more mesic vegetation is found in the pole-facing slopes, while a more xeric vegetation is present on the equator-facing slopes. Since plant characteristics and vegetation assemblages are determined by environmental parameters, replicates of the contrasting vegetation patterns between opposing aspect-slopes are found at north and south hemispheres all around the globe.

[4] The conspicuous effect of aspect on vegetation species composition, distribution, and biomass production [*Coble et al*., 2001; *Desta et al*., 2003; *Liang et al*., 2006; *Bennie et al*., 2008a; *Chmura*, 2008; *Gallardo-Cruz et al*., 2009] is tightly coupled to the local modification of microclimatic variables such as temperature and relative humidity. This microclimatic diversity imposed by topography may reinforce or modify the established ecohydrologic dynamics of a hillslope in favor of determined plant communities or assemblages. For example, in water-limited regions of North America, the modification of microclimatic properties has been found to provide a feedback mechanism inducing the enchroachment of shrubs into grasslands [*D'Odorico et al*., 2010]. Nevertheless, few studies have described the extent to which terrain properties and processes (e.g., aspect, soil development, and vegetative cover) modify the microclimatic regime (e.g., air and soil temperatures, air vapor pressure, energy fluxes, and soil moisture) of opposing slopes, and how these microclimatic modifications may impact hillslope dynamics. In other words, while it is expected that the topographically defined microclimates influence the hydrologic functioning of the hillslopes and ecosystems, detailed quantitative evidence on these relationships is still lacking.

[5] The cooccurrence of distinct ecosystems with sharp and well-defined boundaries in areas of complex topography provide unique opportunities to explore the environmental controls on the dynamics of water and energy fluxes of contrasting ecosystems [*Gutiérrez-Jurado et al*., 2007; *Gutiérrez-Jurado and Vivoni*, 2013a; *Zhou et al*., 2013]. For instance, previous observations in a semiarid catchment of central New Mexico, with opposing slopes and contrasting vegetation, have shown that the particular differences in soil-vegetation-landform properties of the hillslopes result in different soil moisture dynamics within the basin after a large rainstorm [*Gutiérrez-Jurado et al*., 2007]. Specifically, longer soil moisture recession rates were observed on the north facing slope compared to its south facing counterpart. This example provides event-specific evidence of the differential hydrologic response arising from distinct topographic-vegetation conditions. Nevertheless, questions remain regarding whether hydrologic dynamics differ between the slopes over a range of variable meteorological forcings. Specifically, how do the residence times of soil moisture between each ecosystem compare during different seasons of the year? and how would these differences affect the water balance and runoff production of each ecosystem?

[6] Other examples of hydrologic shifts resulting from changes in ecosystem structure exist [*Huxman et al*., 2005; *Turnbull et al*., 2010b; *Nie et al*., 2012; *Vivoni*, 2012]. Some of these efforts have shown that the conversion of grasslands into shrublands leads to the modification of surface processes affecting ecosystem productivity and the spatiotemporal availability of water and nutrients [*Briggs et al*., 2005; *Lett and Knapp*, 2004; *Knapp et al*., 2008; *Turnbull et al*., 2010a, 2010b]. Specific hydrologic processes affected by woody plant enchroachment are rainfall-runoff relations [*Huxman et al*., 2005; *Turnbull et al*., 2010a; *Bedford*, 2008], vertical and lateral infiltration [*Bedford and Small*, 2008], deep percolation and groundwater recharge [*Seyfried et al*., 2005; *Sandvig and Phillips*, 2006], soil deposition and nutrient redistribution and cycling [*Turnbull et al*., 2010b], soil and air temperature regimes [*D'Odorico et al*., 2010] and ecosystem evapotranspiration rates [*Kurc and Small*, 2007] and partitioning [*Wang et al*., 2010]. These shifts in hydrologic processes should be manifested in areas of complex terrain, following natural transitions in vegetation-soil-landform structure. Nevertheless, the extent to which these hydrologic shifts exist and how they impact the seasonal water balances of the ecosystems remain open questions. Elucidating the hydrologic dynamics of these ecosystems as affected by the combined effect of vegetation and topography is crucial for the improvement of land management practices such as soil conservation, ecosystem restoration, and water harvesting in semiarid catchments.

[7] In this study, we conducted a field investigation in a headwater basin of central New Mexico with nearly exact north and south facing slopes and clear vegetation contrasts. Using observations from a network of sensors deployed along slope transects, we quantified the spatiotemporal dynamics of energy and water fluxes of opposing slopes. We address how the observed differences in terrain properties and vegetation cover alter the energy balance of the slopes. We then explore how the topographically mediated energy balance combined with the current ecosystem properties affect water fluxes into and out from the slopes. Our aim is to unveil the underlying mechanisms responsible for the ecohydrologic patterns observed in the opposing slopes of the study basin, and quantify the resulting differences in soil moisture dynamics and water balances of both ecosystems.

[8] This paper is organized as follows. In section 2., we describe the study area, the instrument network, and the techniques used to process and analyze the observations. Section 3. presents results on the topographic modulation of the radiation balance and microclimatic differences between the opposing ecosystems. Next, we analyze the terrain-vegetation effects on the dynamics of soil moisture and quantify the rainfall-runoff relations of the opposing slopes. Then, we examine the effect of energy balance differences on the measured evapotranspiration followed by analyses of soil moisture-evapotranspiration variations between the north and south facing slopes. In section 4., we discuss the implications of the observed energy and hydrologic dynamics on the ecosystem properties and their possible feedbacks to the water balances of the opposing slopes. Finally, section 5. summarizes the study conclusions.

2. Methods

2.1. Study Area

[9] The study area is a headwater basin or catchment ($\sim$0.1 km^2) located in the northwestern corner of the Sevilleta National Wildlife Refuge in central New Mexico (Figure 2). The climate in the area is semiarid with a mean annual temperature of 20°C and two distinct rainy seasons: a summer monsoon with high intensity, short duration events accounting for $\sim$60% of the annual rainfall, and lower intensity frontal systems with occasional snow precipitation contributing the remaining $\sim$40% of the annual rainfall distributed within the winter and spring months [*Milne et al*., 2003]. The basin is part of a set of displaced alluvial fans of Plio-Pleistocene origin, giving rise to a series of nested basins with various degrees of incision and characteristic vegetation contrasts resulting from different hillslope aspects. Vegetation structure and composition in the basin is clearly associated to variations in aspect, from which essentially two ecosystems are defined: a mesic, juniper-grass savanna on the north facing slope (NFS), and a xeric, creosote shrubland on the south facing slope (SFS). In this basin, the east facing slope (EFS) acts as the ecotone between the NFS and SFS ecosystems. Vegetation composition in the NFS is dominated by one-seed junipers (*Juniperus monosperma*; 20% cover) in association with hairy and black gramma (*Bouteloa spp.*; 21% cover), while in the SFS, creosote (*Larrea tridentata*; 7.8% cover), mariola (*Parthenium incanum*; 6.6% cover), fluff grass (*Erionuron pulchellum*; 7% cover), and slim tridens (*Tridens muticus*; 6% cover) are the keystone species [*McMahon*, 1998].

[10] The soils of the study area are forming in coarse fan gravels with a sandy matrix and calcium carbonate ($CaCO_3$) horizons formed in a predominantly horizontal orientation. With the incision of drainages into these fan gravels, the modern aridisol soil with calcic horizons form parallel to the slope, and the older horizontal calcic horizons intersect the current hillslope profile at various locations. The presence, depth, and stage of induration of the $CaCO_3$ layers in the soils vary according to aspect and reveal differences in the magnitude and direction of soil moisture fluxes among the slopes. As a result, the hydrology of the study basin is strongly influenced by the distinct properties of the soils of three slopes with different aspects [*Gutiérrez-Jurado et al*., 2006]. For example, NFS soils have higher percentages of fines (i.e., silts and clays), organic matter and $CaCO_3$, as compared to SFS and EFS soils. In addition, the depth to the $CaCO_3$ on the NFS soils is greater than that of the SFS soils, indicating deeper infiltration fronts on the NFS [see *McMahon*, 1998; *Gutiérrez-Jurado et al*., 2006]. The soils of the headslope (EFS) do not follow the same patterns of the NFS and SFS soils. The EFS soils are well drained with decreasing $CaCO_3$ accumulation and at a greater depth along the downslope direction of the headslope suggesting a greater moisture flux toward the toe of the slope.

2.2. Instrument Network

[11] A network of instruments was deployed in the study basin to quantify the effect of terrain and vegetation in the dynamics of water and energy fluxes of the slopes. The instruments are grouped by systems and include: Bowen

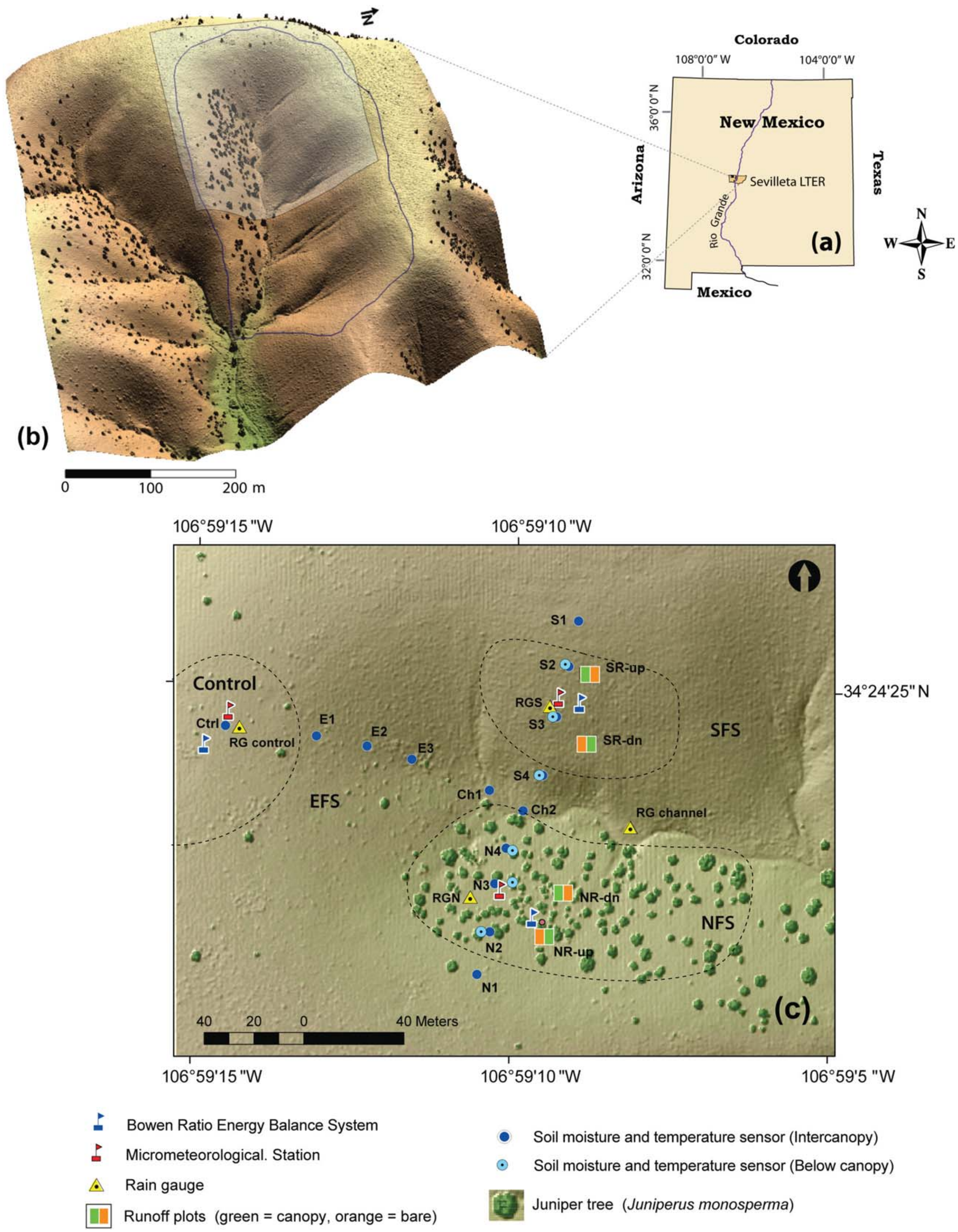

Figure 2. (a) Location of the Sevilleta National Wildlife Refuge in New Mexico; (b) 3-D view of the study catchment with its boundary denoted by a blue line, showing the juniper trees as black dots; and (c) location of instruments (shaded area in Figure 2b). The nomenclature of the sensors for each $\theta - T_s$ transect are identified with an N for the NFS, S for the SFS, and E for the EFS, followed by a number indicating the position within the slope and decreasing in the upslope direction. Figures 2b and 2c were produced using a 0.5 m resolution Digital Elevation Model derived from airborne LiDAR courtesy of the National Center for Airborne Laser Mapping.

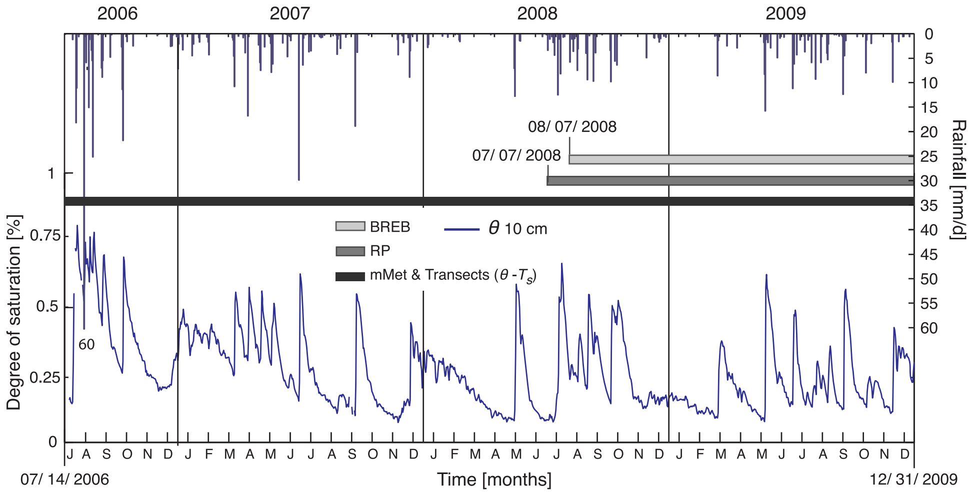

Figure 3. Daily shallow soil moisture, expressed as a degree of saturation (%) and rainfall at the Control site during the study period. The horizontal bars show the availability of data.

Ratio Energy Balance systems (BREB), micrometeorological stations (mMet), soil moisture (θ), and soil temperature (T_s) transects ($\theta - T_s$), and runoff plots (RP). Figure 2c shows the location of the instruments obtained via a differential global positioning system (dGPS) survey. The arrangement of the instruments was designed in a way that permits the analysis of differences between the NFS and SFS by: (1) direct comparison of their data and (2) by benchmarking the data to a control location (Control) in the upper flat surface above the EFS. As a result, the instrument systems are arranged as follows: there is a BREB and a mMET in each of the NFS, SFS, and Control; there is one $\theta - T_s$ per slope (NFS, SFS, and EFS) and three additional θ and T_s sampling locations at the Control, and two channel locations; there are two sets of RP (2 runoff plots per set) for the NFS and SFS; finally, there are four rain gauges distributed in the basin. In addition, to minimize any potential uncertainties inherent to the methods used in the measurement of the variables, we placed special attention to the location of the instruments within the slopes, particularly for the BREB, mMet, and θ and T_s transects. The BREB and mMET stations of the NFS and SFS were placed at a mid-slope location to ensure a sufficiently large fetch within the slopes and reduce potential cross-contamination problems between the slopes (Figure 2c). The θ and T_s were deployed in vertical transects going from the top to the bottom of the slopes to assess the effect of slope position on moisture dynamics (Figure 2c). Detailed descriptions of the instrument systems are given in the following subsections. All data from the network of sensors has been subject to strict quality control procedures, including the inspection of anomalous records (values exceeding ± 2 standard deviation) and their removal when appropriate.

2.3. Study Period and Data Availability

[12] The period of observations is shown in Figure 3, along with time series of daily rainfall and 10 cm depth mean daily θ at the Control. Note that data availability varies with instrument system. The longest period of data availability (~3.5 years) correspond to the mMets and $\theta - T_s$ (14 July 2006 to 31 December 2009), followed by the RP sets (7 July 2008 to 31 December 2009) and the BREB systems (7 August 2008 to 31 December 2009) with little less than ~1.5 years of data. The study period commences in the middle of a wet summer in 2006 [*Gutiérrez-Jurado et al*., 2007] when a sequence of large storms sustained θ at levels above field capacity during the remaining part of the season. Soil moisture at the monitored depths from these events was not completely depleted until a year later. During the observations, the basin underwent characteristic wetting periods during the summers from monsoonal rains and rewetting occurred between the late fall to early winter with dry episodes in between. It is also noteworthy to observe the rapid θ recessions for summer wetting events as opposed to the slow winter θ recessions, suggesting a seasonal control on the depletion rates of θ. Further analyses of θ, energy balance and micrometerological variables exploring these seasonal effects are presented subsequently.

2.4. Soil Moisture and Soil Temperature Measurements

[13] Volumetric soil moisture and soil temperature were measured at two depths (10 and 20 cm) at 6 canopy and 12 intercanopy patches, and 2 locations along the channel using Campbell Scientific CS-616 water content reflectometers (WCRs) and 107 L temperature probes, respectively. WCR and 107 L probes were placed in pairs parallel to the surface at each monitoring location and depth. θ and T_s were measured at 1 min intervals and 30 min averages were recorded. WCRs measure the dielectric permittivity (in mV) of the soil which is a function of the moisture content. Sensor outputs (mV) were converted to volumetric soil moisture using a gravimetric calibration procedure. Due to soil heterogeneity and gravel content, site-specific calibration was performed during various dates to determine gravimetric moisture content, dry bulk density, and soil porosity, on all locations except at E3, CH1, S2, cS1, and S4. For these locations, parameters from the nearest site were used and tested for consistency. The 107 L temperature probes do not require calibration. In this study, we

report values of volumetric soil moisture in (m^3/m^3), referred to as θ, and soil moisture degree of saturation in (%) referred to as θ_s. Soil saturation water content was determined from porosity values obtained via soil sampling and laboratory analyses. The values for T_s are reported in °C.

2.5. Micrometeorological Measurements

[14] Micrometeorology variables were measured on the NFS, SFS, and Control locations at 30 min intervals using standard weather stations from Campbell Scientific: relative humidity (RH) in (%), air temperature (T_a) in (°C), windspeed (μ) in (m s^{-1}), wind direction (*WD*) in (degrees), rainfall (*P*) in (mm), and incoming shortwave radiation (SW_{in}) in (W m^{-2}). To investigate the effect of topography on the microclimatic differences of the opposing slopes, we performed comparative analyses using time series of mean daily values for T_a, μ, and vapor pressure deficit (*VPD*; calculated using RH and T_a after *Dingman* [2000]).

2.6. Runoff Measurements

[15] Runoff was measured using runoff plots (RPs) deployed on the north and south facing slopes. The RPs consist of 4 × 2 m exclusion plots connected to a flume where flow depth is measured using a Global Water WL400 pressure transducer located inside a stilling well. The fiberglass flumes are of the HS type [*Brakensiek et al.*, 1979]. In each plot, runoff is collected in PVC tubes then funneled down a 0.6 m long chute sloped at 2° to the flume [*Gwinn*, 1984]. Plot walls are buried 0.1–0.15 m deep depending on terrain conditions. Water depth values were converted to discharge (Q_s) using a quadratic equation derived from rating curves [*Gwinn and Parsons*, 1976]. Q_s values were subject to quality control procedures to remove the effect of sensor drift and sensor malfunction.

2.7. Energy Balance and Bowen Ratio Measurements

[16] The energy balance at the land surface is described as

$$R_n = G + H + \lambda E, \tag{1}$$

where R_n is the net radiation on the surface in (W m^{-2}), G is the soil heat flux in (W m^{-2}), H is the sensible heat flux in (W m^{-2}), and λE is the latent heat flux in (W m^{-2}). In this study, we measured R_n and G directly and calculated H and λE using the Bowen ratio (β) method [*Bowen*, 1926].

[17] The four components of the radiation balance, namely the incoming shortwave (SW_{in}), outgoing shortwave (SW_{out}), incoming longwave (LW_{in}), and outgoing longwave (LW_{out}), were measured on the NFS, SFS, and Control with CNR1 net radiometers. The radiometers were installed horizontally at ~2 m height from the ground and away from any nearby obstruction. Because the radiometers were placed horizontally, corrections to account for the slope and aspect effects were performed following the method by *Tian et al*. [2001] as described in Appendix A.

[18] Soil heat flux density was measured at 5 cm depth below canopies and bare soil patches at each BREB location following a calorimetric-based approach [*Fritschen and Simpson*, 1989]. In this method, G is obtained by adding the soil heat flux (G_p) at a reference depth to the change in energy stored in the soil layer above the reference depth [*Kimball et al*., 1976]. Site-averaged values for each location were calculated based on the weighted percent cover of canopy versus bare soil following *Kurc and Small* [2004].

Table 1. Deployment Set Up for Each Bowen Ratio Energy Balance System

BREB System	AEM Separation Distance (m)	Lower Arm Height (m)	Average Canopy Height[a] (m)
Control	1.05	0.5	0.2
NFS	1.65	2.2	1.7
SFS	1.66	0.86	0.4

[a]Average canopy height was estimated from individuals within a 5 m radius.

[19] β is the ratio of sensible heat (H) flux to latent heat (λE) flux:

$$\beta = \frac{H}{\lambda E} = \frac{P \cdot c_a \cdot dT_a/dz}{(\lambda \cdot \varepsilon) \cdot de/dz}, \tag{2}$$

where P is atmospheric pressure (kPa) at a constant height, c_a is the air heat capacity (MJ kg^{-1} K^{-1}), λ is the latent heat of vaporization in (MJ kg^{-1}), ε is the ratio of the gas constants for air and water vapor with a value of 0.622, dT_a/dz is the change in air temperature (T_a) with height (z) (°C m^{-1}), and de/dz is the change in air vapor pressure (e) with height (z) (kPa m^{-1}). We used temperature and humidity probes mounted on an Automated Exchange Mechanism (AEM) that switches the vertical location of the probes to eliminate potential bias on the sensors readings due to condensation and heating effects [*Fritschen and Simpson*, 1989]. The setup of the vertical probes is described in Table 1, while the approximate fetch is shown in Figure 2c with dotted lines. The approximate fetch of each BREB system (Figure 2c) was calculated following *Nie et al*. [1992], based on the height of the instruments, vegetation height, and the prevailing wind direction for each location.

[20] Measurements of β can be combined with the energy balance to obtain λE and H as

$$\lambda E = \left(\frac{R_n - G}{1+\beta}\right), \tag{3}$$

$$H = \beta \cdot \lambda E = \frac{\beta(R_n - G)}{(1+\beta)}. \tag{4}$$

[21] Each of the components of β and the energy balance were subject to strict quality control procedures. Errors in the quantified fluxes inherent to the BREB method for arid conditions were found and discarded following the method by *Pérez et al*. [1999]. The resulting values for each of the four energy balance components were examined for consistency (i.e., $R_n - G \approx H + \lambda E$). Comparisons with values obtained in other locations of similar characteristics yielded good agreement [*Kabat*, 1997; *Kurc and Small*, 2004]. Finally, to examine the causes of differences in latent heat flux among the three locations, we calculated and report

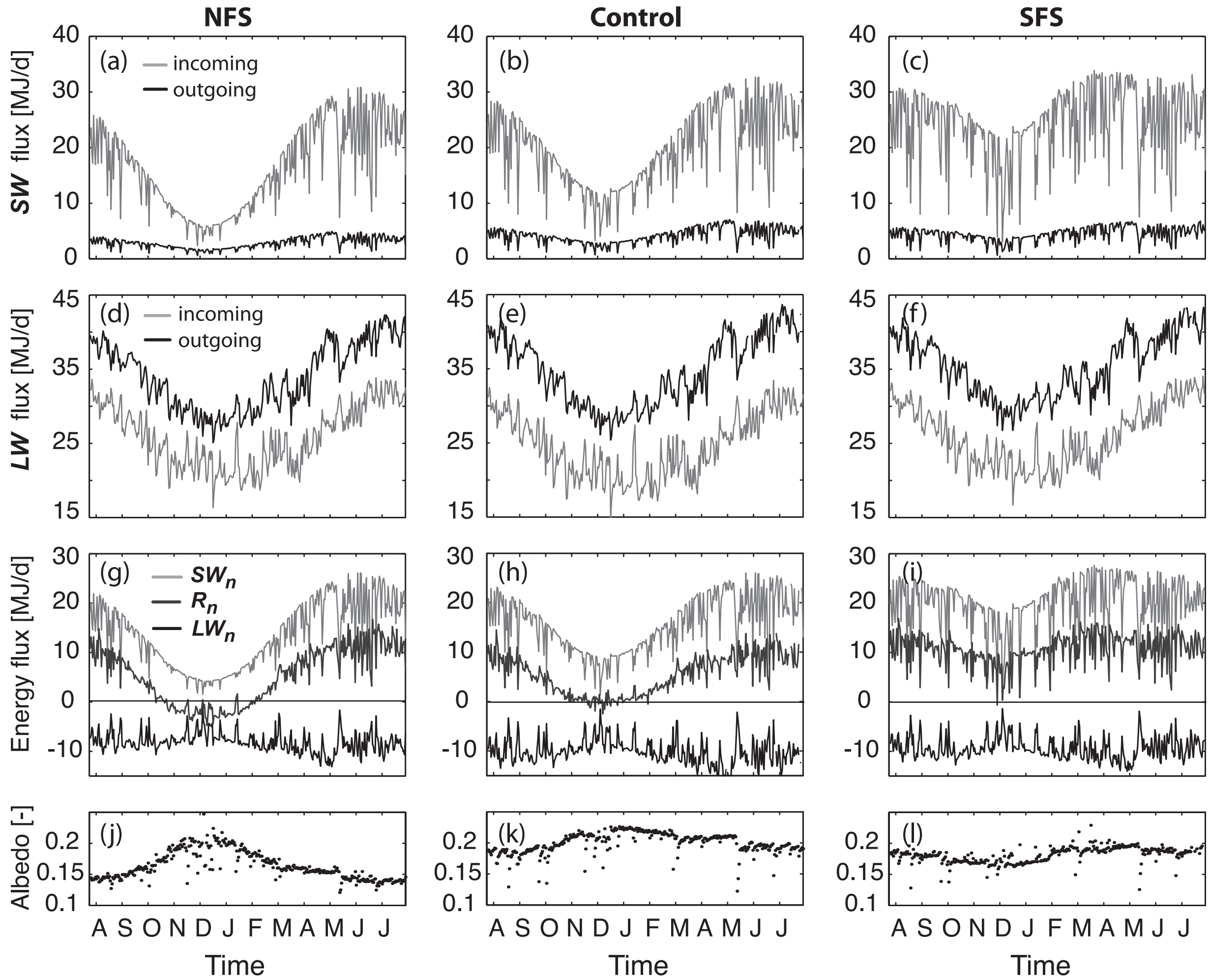

Figure 4. Intraannual variation of the radiation balance components for each BREB location: (a–c) the shortwave components; (d–f) the longwave components; (g–i) the R_n, SW_n, and LW_n components; and (j–l) the variation in albedo.

values of midday (between 10:00 A.M. and 4:00 P.M.) available energy ($R_n - G$) and midday average values of the evaporative fraction (EF), obtained as

$$EF = \frac{1}{1+\beta}. \quad (5)$$

3. Results

3.1. Topographic Modulation of the Radiation Balance

[22] The annual cycle for each radiation component is shown in Figure 4. Incoming shortwave radiation (SW_{in}) shows the largest differences between all radiation components among the three locations. The annual cycle of SW_{in} shows a strong sinusoidal pattern with the highest values during the summer months and the lowest during the winter months. As compared to the Control, the seasonal variation in SW_{in} at SFS is dampened, while on the NFS, it is greatly amplified. Because in all cases SW_{out} is small compared to SW_{in}, and since LW_n is relatively constant during the year, the resulting net radiation (R_n) preserves the same pattern of SW_{in}. As a result, during the lowest SW_{in} period from mid-October to late February, the daily R_n for the NFS is negative (<0 MJ/d), for the Control is close to zero, and for the SFS remains positive and high (~7–8 MJ/d). This topographic modulation of the seasonality in R_n is also reflected in the albedo of the three locations. Specifically, the NFS has a strong increase in albedo during the winter months, while a slight increase is noted for the Control, and a slight decrease occurs for the SFS. Overall, the general patterns show that north facing slopes enhance seasonal differences in the radiation components, especially during the fall and winter periods, while the south facing slopes dampen the seasonal variations of incoming shortwave and net radiation. These results suggests that radiation differences resulting from increased (reduced) seasonal variability in north (south) facing slopes act as a main driver of the ecohydrologic processes occurring in the opposing slopes.

3.2. Topographic Modulation of Microclimate

[23] Figure 5 shows the mean monthly rainfall and corresponding standard deviations for each rain gauge in the study basin. Although the period of record is relatively limited (~3.5 yrs), a number of temporal rainfall patterns can be recognized. For instance, the largest proportion of the

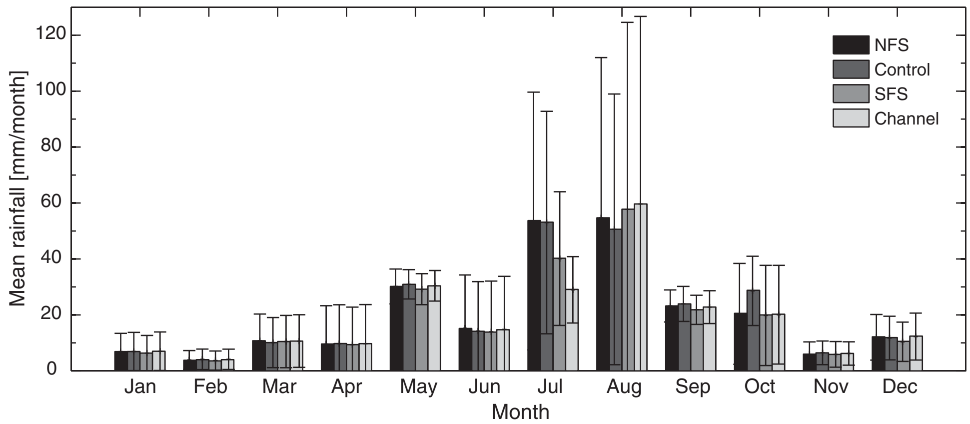

Figure 5. Mean monthly rainfall for each rain gauge in the study basin. The vertical lines show ± the standard deviation in monthly rainfall.

annual precipitation falls in the months between May to October, while the mean monthly rainfall during the rest of the year is less than 15 mm and exhibits low interannual variability. The influence of the North American monsoon can be clearly observed with the mean monthly averages for July and August above 50 mm. Generally, mean monthly rainfall values for all the locations in the basin are very similar. Nevertheless, there can be substantial differences in mean monthly rainfall among the four locations during the summer months. This is particularly pronounced for the month of July, when differences among all locations are largest, and in some instances can account for as much as 50% difference in rainfall. It is possible that these differences are related to a combination of rainfall directionality with topographic sheltering [*Ivanov et al*., 2008b].

[24] To investigate the effect of topography on the microclimate of the opposing slopes, we present the differences (Δ) of the NFS and SFS with respect to the Control (e.g., Δ_{NFS} = NFS − Control, and Δ_{SFS} = SFS − Control) of the mean daily values for the following variables in Figure 6: air temperature ($\overline{T_a}$, in (°C)), shallow (10 cm) soil temperature ($\overline{T_s}$, in (°C)) at the midslope intercanopy (N3 and S3) locations, vapor pressure deficit ($\overline{VPD}$, in (% difference)), and wind speed ($\overline{\mu}$, in (% difference)). To show the canopy effect on $\overline{T_s}$, a 15 day moving average of locations cN3 and cS3 was also included. Finally, to serve as a reference, Figure 6a shows the time series of daily SW_{in} at the Control for the study period. To best show the differences between Δ_{NFS} and Δ_{SFS}, note that VPD and μ plots are shown as percent difference. For $\overline{T_a}$, $\overline{T_s}$, and $\overline{VPD}$, there is an apparent seasonal effect on Δ_{NFS}. Δ_{NFS} in $\overline{T_a}$ and $\overline{VPD}$ follow closely the variations in SW_{in}, reaching peak (positive) values in the summer months and their lowest (negative) values during the late fall and winter months. On the other hand, Δ_{SFS} in $\overline{T_a}$ and $\overline{VPD}$ do not follow similar seasonal patterns. Instead, Δ_{SFS} in $\overline{T_a}$ shows an overall negative trend, with positive values through the first year and half and negative values in the last year of data, while Δ_{SFS} in $\overline{VPD}$ shows consistently positive values, fluctuating around 8% difference. In a similar manner, Δ_{NFS} in $\overline{\mu}$ and Δ_{SFS} in $\overline{\mu}$ do not follow a seasonal pattern, but rather show consistently negative values, which fluctuate around −20% for Δ_{SFS} in $\overline{\mu}$ and −50% for Δ_{NFS} in $\overline{\mu}$. Perhaps the best illustration of the modulating effect of topography are the variations in $\overline{T_s}$. Both Δ_{NFS} and $\Delta_{SFS} in \overline{T_s}$ show a strong seasonal signal but with opposite effects, with negative (Δ_{NFS}) and positive (Δ_{SFS}) differences growing toward the winter months and decreasing to zero when approaching the summer months. It is worth noting that during large periods of the winter, the difference in $\overline{T_s}$ between Δ_{NFS} and Δ_{SFS} can be as large as 10°C. Also, note the different effects of canopy cover on the opposing $\overline{T_s}$ with respect to the Control. Specifically, the juniper canopy in the NFS dampen the seasonal signal by preserving Δ_{NFS} more or less constant (∼−3°C), while the creosote canopy in the SFS follows the same seasonal pattern of the intercanopy Δ_{SFS}.

3.3. Soil Moisture and Temperature Dynamics of the Opposing Slopes

[25] We conducted a series of analyses using the soil moisture and temperature observations to quantify the differences in the root zone (∼0–25 cm) dynamics in the opposing slopes. Figure 7 presents soil moisture shown as degree of saturation (θ_s) for five representative locations within the study basin and the rainfall variations at the Control site. The dynamics of θ_s reveal a clear drying trend for the study period. This trend is stronger at the Control and NFS locations, since soils at these sites preserve the moisture pulses from the 2006 summer and 2006–2007 winter rains for a longer time. Comparing the intercanopy (θ_{si}) and canopy (θ_{sc}) data, we notice a different response of soil moisture to varying amounts of rainfall between the soils under the juniper canopies on the NFS and those under creosote shrub canopies on the SFS. On the NFS θ_{sc} shows little or no response to small rainfall events (i.e., <10 mm/day), suggesting that intercepted water by the juniper canopies is lost to evaporation. On the other hand, θ_{sc} on the SFS shows responses even for short amounts of rainfall (i.e., <3 mm/day) that θ_{si} does not capture, pointing to the possibility of stemflow funneling within creosote shrub canopies similar to observations by *Martínez-Mesa and Withford* [1996]. Other possible explanations to this differential moisture response under the shrub canopies to small rainfall events are the effect of the canopy in reducing the raindrop impact [*Bergkamp*, 1998], and the plants ability on modifying the properties and structure of the soil, all of

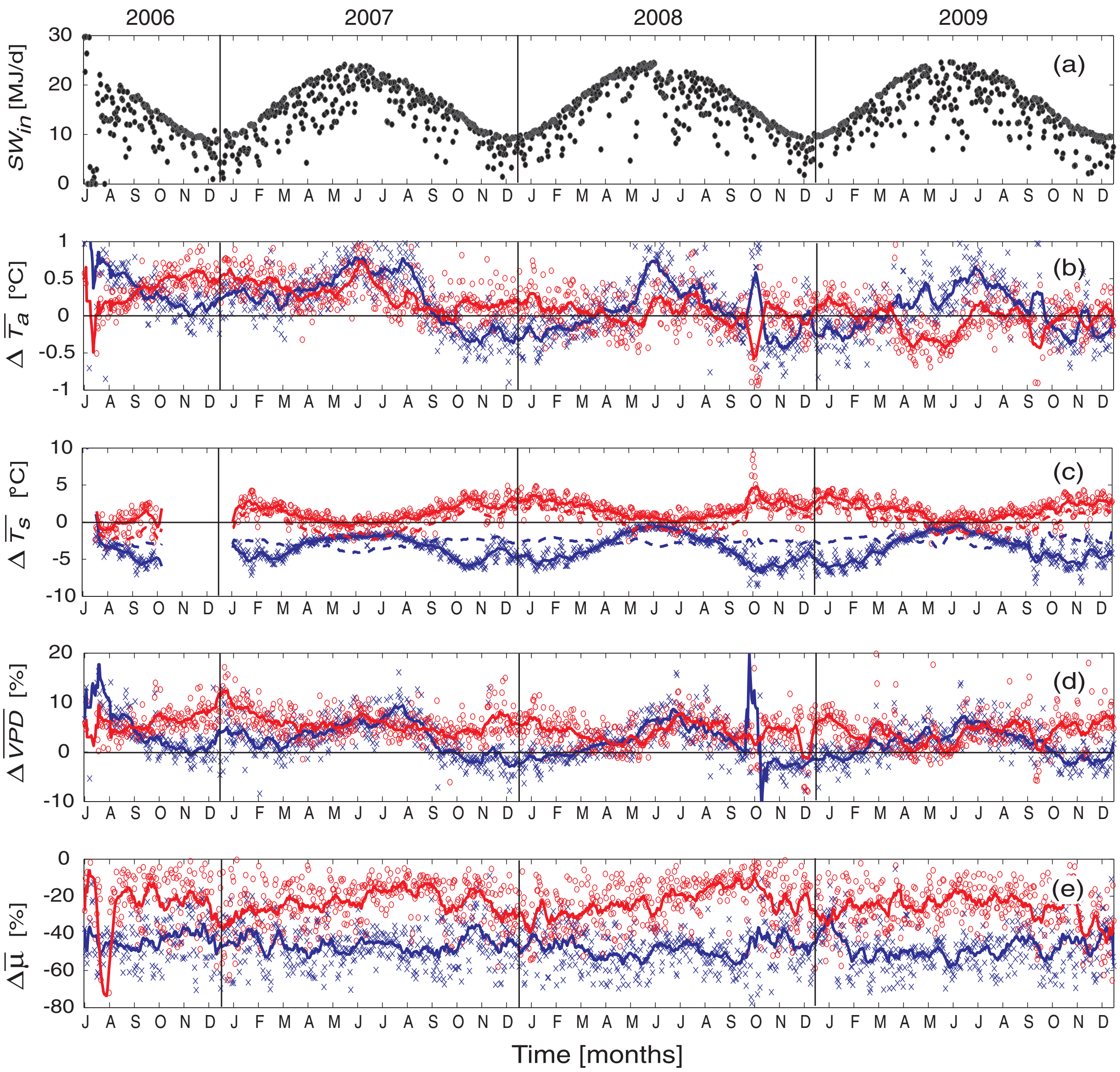

Figure 6. Comparative time series of micrometeorological variables from NFS (blue crosses) and SFS (red circles) with respect to the Control. (a) Incoming shortwave radiation (SW_{in}) at Control; (b) difference in mean daily air temperature ($\Delta\overline{T_a}$) in (°C); (c) difference in mean daily shallow (10 cm) soil temperature ($\Delta\overline{T_s}$) in (°C); (d) percent (%) difference in mean daily vapor pressure deficit ($\Delta\overline{VPD}$); (d) percent (%) difference in mean daily wind speed ($\Delta\overline{\mu}$). The solid lines show a 15 days moving average, while the dotted lines in Figure 6c are 15 days moving averages for $\Delta\overline{T_s}$ at canopy sites.

which are known to enhance infiltration [*Perkins and McDaniel*, 2005]. For example, *Devitt and Smith* [2002] noted that creosote shrub roots increase soil permeability and porosity allowing for faster and deeper infiltration, as a result of secondary porosity created by dead roots within the soil. On the EFS and SFS sites, Figures 7c and 7e show negligible differences in the response of soil moisture between 20 and 10 cm depth for all rainfall amounts, suggesting similar infiltration properties within the first 20 cm of the soil at both locations. On the other hand, the θ_s at the Control and NFS sites show differences between the observations at 10 and 20 cm for moderate-to-low rainfall events, with a highly responsive θ_s at 10 cm and slight to nonresponsive 20 cm θ_s. These observed differences in soil moisture responses with depth in the opposing slopes indicate varying infiltration characteristics, which should be reflected in distinct rainfall-runoff patterns that will be explored in a subsequent section.

3.3.1. Topographic-Vegetation Effects on Soil Moisture Residence Times

[26] In semiarid ecosystems, the time window of water availability after wetting events is critical for plant water use [*Loik et al.*, 2004; *Schwinning and Sala*, 2004]. Therefore, understanding the dynamics and characteristics of soil moisture recession of the opposing slopes will provide insights into the observed contrasts in vegetation cover. In the opposing ecosystems of our study basin, the differences in soil properties and energy balance should be manifested

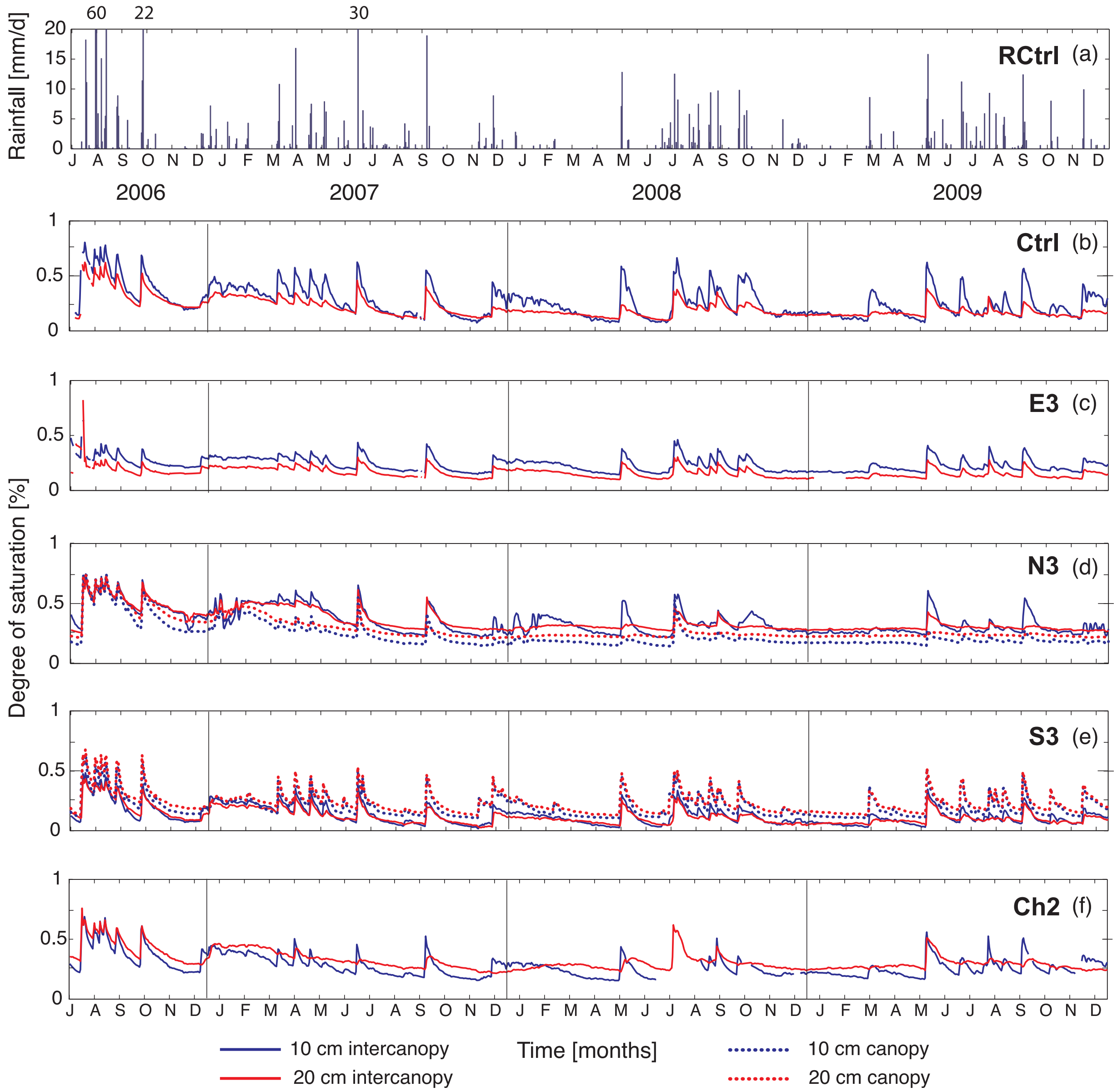

Figure 7. (a) Rainfall and (b–f) soil moisture at 10 cm (blue lines) and 20 cm (red lines) depths, at intercanopy (solid lines) and canopy (dotted lines) locations. The soil moisture is shown as degree of saturation ($\theta_s = \theta/n$, where θ is volumetric water content and n is porosity) in percent (%).

in different soil moisture recessions for distinct parts of the year. Time constants for soil moisture recession (i.e., soil moisture residence times) were obtained by calculating the time at which there is a 63% decrease in moisture content after a substantial infiltration event (typically after a >7 mm rainfall), following a method used by *Kurc and Small* [2004]. Figure 8 shows seasonal averages of soil moisture recession time constants (τ) for different sampling locations. In general, soil moisture residence times vary significantly with season, aspect and slope position, and between intercanopy and canopy locations at 10 cm depth. For example, during the summer, τ is on average 2 days longer for the north facing slope as compared to the south facing slope at the same slope positions. Differences between SFS and NFS τ decrease notably during the fall when all intercanopy τ approximate the value at the Control site. Interestingly, the largest differences between NFS and SFS occur during the spring, with τ diverging by as much as 5 days between the top slope positions at the NFS and SFS. In addition, the spring exhibits the largest differences in τ with slope position in each ecosystem. For instance, τ differences for the top and bottom locations on the EFS and SFS are as large as ~4.5 days, while differences for the same locations along the NFS are ~3.5 days. In general, the effect of the canopies on the dynamics of soil moisture is to reduce τ, with the largest differences between canopy and intercanopy sites occurring during the spring. In summary, a strong control of seasonality and slope position is observed on the dynamics of τ that can be related to the expected variations in evapotranspiration and drainage.

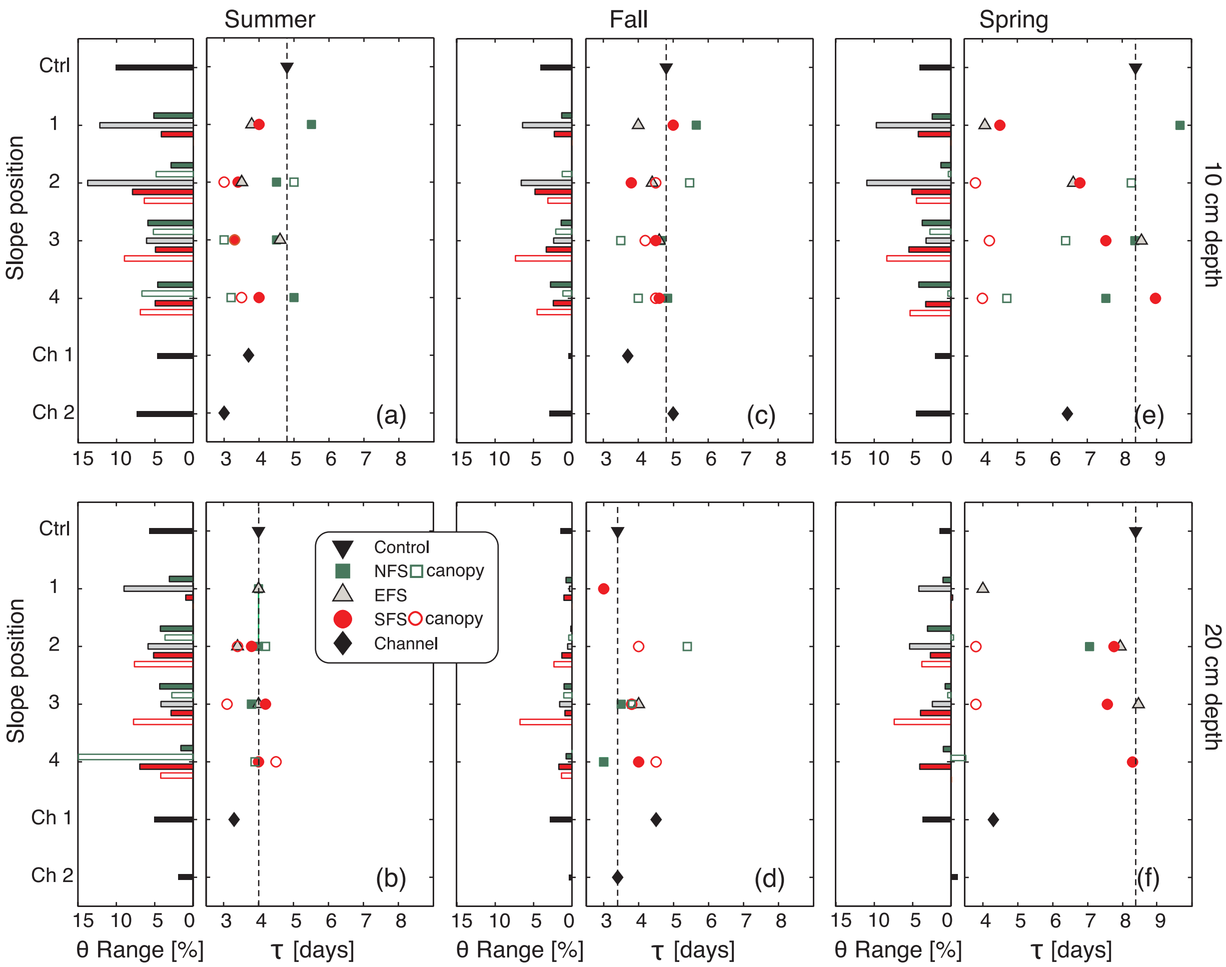

Figure 8. Soil moisture residence times (τ) in (days) and their corresponding θ range in (%) for all the sampling locations, organized by seasons and soil depth. The range is defined as the maximum difference in soil moisture within the season. The coloring of the bars showing the volumetric θ range follows the same order of their symbol counterparts. The dashed line indicates the Control residence time.

3.3.2. Temporal Stability of Soil Moisture and Temperature

[27] To examine the terrain (slope-aspect-soils) and vegetation effects on the long-term spatial patterns of θ and Ts, we performed temporal stability analyses for the $\theta - T_s$ transects, following a similar approach to *Lin* [2006] and *Martínez-Fernández and Ceballos* [2003]. We calculated the time average $(\overline{\delta_i})$ of the relative difference for the mean daily θ_s $(\overline{\delta_i}(\overline{\theta_s}))$ and mean daily T_s $(\overline{\delta_i}(\overline{T_s}))$ with respect to the Control, as follows

$$\overline{\delta_i} = \frac{1}{m}\sum_{j=1}^{m}\delta_{ij}, \tag{6}$$

$$\delta_{ij} = \frac{v_{ij} - v_{Ctrl \cdot j}}{v_{Ctrl \cdot j}}, \tag{7}$$

where m is the number of monitoring days, δ_{ij} is the value of the variable υ (i.e., $\overline{\theta_s}$ or $\overline{T_s}$) at a given depth, at site i, and on measurement day j, and $v_{Ctrl \cdot j}$ is the value of the variable at the Control. For these analyses, positive values of $\overline{\delta_i}(\overline{\theta_s})$ $(\overline{\delta_i}(\overline{T_s}))$ indicate higher $\overline{\theta}_s$ $(\overline{T}_s)$ values year round relative to the values at the Control; likewise, negative $\overline{\delta_i}(\overline{\theta_s})$ indicate lower $\overline{\theta}_s$ values than those at the Control. Additionally, the standard deviation (σ) for each $\overline{\delta_i}$ was calculated as a way to identify the most time stable locations (i.e., lowest $\sigma(\delta_i)$).

[28] Figure 9 presents joint $\overline{\theta}_s$ and $\overline{T}_s$ time stability plots, showing $\overline{\delta_i}(\overline{\theta_s})$ versus $\overline{\delta_i}(\overline{T_s})$ and their corresponding $\sigma(\delta_i)$ for 10 cm and 20 cm soil depths for all sampling locations. Each point is labeled with numbers relative to their slope position. The analysis clearly illustrates the effect of topographic location and vegetation cover on the temporal stability of $\overline{\theta}_s$ and $\overline{T}_s$. There is a clear progression in $\overline{\delta_i}(\overline{\theta_s})$ and $\overline{\delta_i}(\overline{T_s})$ values from NFS to EFS and SFS locations. The NFS sites are located at the wetter and cooler regions (upper left quadrant), while SFS sites are located in the drier and warmer portions of the diagram (lower right quadrant). EFS sites are found at locations intermediate to the NFS and SFS. These results are consistent with the transition in vegetation type (i.e., mesic to xeric), and soils documented by *McMahon* [1998] and *Gutiérrez-Jurado et al.* [2006].

[29] In general, the temporal stability plots reveal less stable (larger $\sigma(\delta_i)$) and more clustered data points for each group (i.e., NFS, EFS, SFS) at 10 cm than at 20 cm. This is

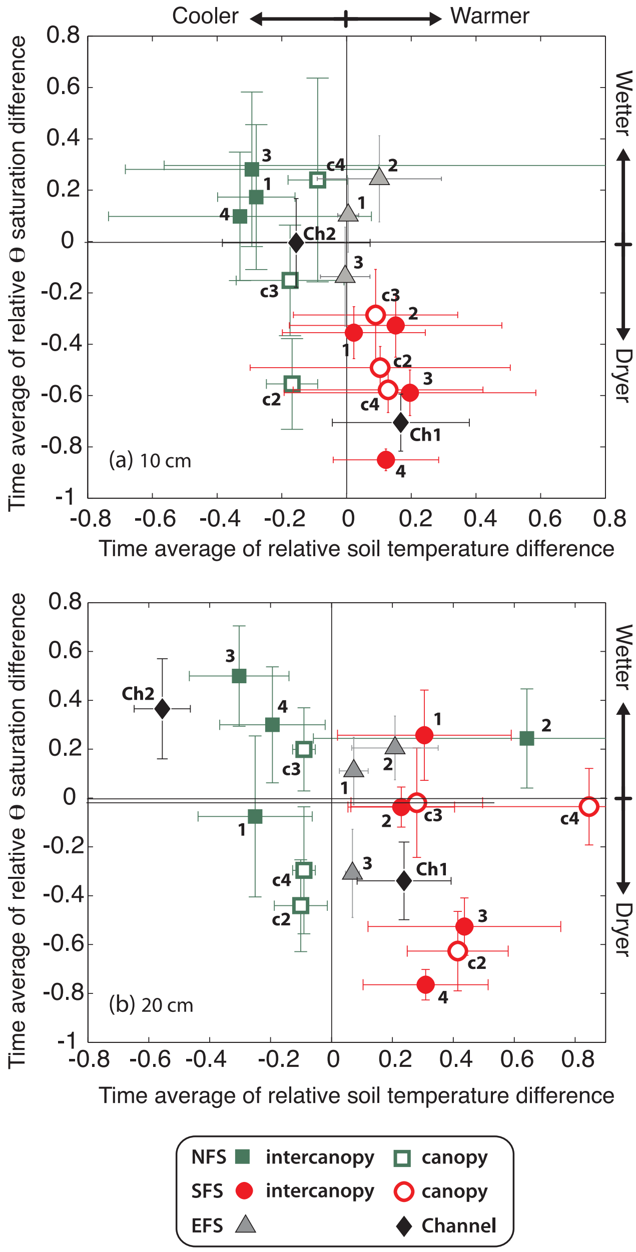

Figure 9. Joint temperature and soil moisture time stability diagrams for (a) 10 cm and (b) 20 cm soil depth for all sampling locations. Numbers next to data points indicate slope location. Vertical lines show ± one standard deviation in $\overline{\delta_i(\overline{\theta_s})}$ and the horizontal lines show ± one standard deviation in $\overline{\delta_i(\overline{T_s})}$. All points are plotted relative to the temperature and θ values of the Control location (i.e., 0,0 coordinate in the plots).

an indication that the soils become more hydrologically heterogeneous going deeper into the root zone. Interestingly, the EFS and intercanopy SFS data points exhibit some spatial organization for both $\overline{\theta}_s$ and $\overline{T}_s$ within the slope that is preserved at both depths. In the SFS intercanopy locations, the soils become drier progressing from the top to the bottom of the slope, and preserve the same pattern in $\overline{\delta_i}(\overline{T}_s)$. In the EFS, there appears to be a transition from a top location (E1) that is similar to the Control to variable conditions further downslope (E2 and E3). In contrast, the effect of slope position on the NFS locations is overridden by the heterogeneity imposed by vegetation. Note the stabilizing influence of juniper canopies on the consistency of soil temperature for both depths (Figure 9). Furthermore, an interception effect is also apparent, with two of the three canopy locations at both depths permanently drier than the Control and the other NFS locations (Figure 8). Additional support to this statement is observed in Figure 7d, where soil moisture under the canopy shows no response to various precipitation events, including a number of large rainfalls (>15 mm/d). Finally, the channel locations exhibit markedly different $\overline{\theta}_s$ and $\overline{T}_s$ behaviors. While the channel head (Ch1) clusters well with the SFS locations in the warmer and drier quadrant, the channel bank (Ch2) resembles more the NFS intercanopy locations, suggesting a potential connectivity between each slope and differing sections of the channel.

3.4. Runoff Response of the Opposing Slopes

[30] We present a suite of analyses to characterize the differential runoff (Q) responses to rainfall (P) in the opposing slopes. Tables 2 and 3 present the runoff event characteristics at each runoff event recorded at each runoff plot (RP) during the study period. Figure 10 summarizes Q for intercanopy and canopy plots in each slope using a number of different metrics. The runoff ratio (Q/P) is used to depict the amount of precipitation converted into runoff. For the majority of the runoff events recorded on the NFS, 13% of P was converted into runoff ($Q/P \leq 0.13$), and Q/P exceeded 20% only a few times. For the SFS plots, on the other hand, half of the events had $Q/P \leq 0.1$, while the other half varied between 0.1 and 0.7 depending on location within the slope and canopy cover. The differences in Q/P between the opposing slopes and categories are consistent with the total amounts of runoff ($\sum Q_T$) during the study period. At the annual scale, Q/P differs between the opposing slopes by at least one order of magnitude, with NFS values ranging between 10^{-3} and 10^{-4}, and SFS values ranging between 0.01 and 0.07. On the SFS plots, $\sum Q_T$ was 5–6 times higher than on the NFS plots. Similarly, SFS plots recorded a larger number of runoff events than NFS plots; the highest Q frequency was registered on the SFS canopy plots (20 events), followed by the SFS intercanopy plots (15 events), the NFS intercanopy plots (10 events), and finally the NFS canopy plots (6 events). Within each slope, the differences in $\sum Q_T$ between canopy and intercanopy plots were relatively minor, ∼10% for the SFS plots and ∼25% for the NFS plots, and primarily confined to the upslope plots. Notably, in all the cases, $\sum Q_T$ was considerably higher on the upslope plots, partly as a result of higher frequency of Q except for the NFS canopy plot, where the downslope plots recorded more runoff events.

[31] Figure 10 also shows the relationship between total event precipitation (P_E) to the time lag to runoff peak (T_{LP}), and to runoff peak (Q_P). Although the relationship between P_E and T_{LP} exhibits variability, there seems to be a threshold-like pattern of response between these two variables. For very large P_E ($\geq$10 mm), there is a consistent and almost constant response in T_{LP} (10 min). The relation between P_E and Q_P is quite variable for the SFS plots, but a

Table 2. Characteristics of Recorded Runoff Events on the NFS During the Study Period[a]

	Plot Type		Date (mm/dd/yyyy)	P_E (mm)	T_{LP} (min)	Q_T (L)	Q_P (L/s)	Q/P
NFS	Upslope	c	7/18/2008	12.5	7.3	24.1	0.129	0.22
		c	9/09/2008	10.1	8	4.3	0.019	0.05
		int	7/18/2008	12.5	7.3	6.1	0.04	0.06
		int	8/29/2008	3.8	0.3	6.9	0.009	0.21
		int	9/09/2008	10.1	8.2	5.3	0.03	0.06
		int	5/22/2009	3.3	39.5	1	0.002	0.04
		int	5/23/2009	5.1	50	1.3	0.002	0.03
		int	5/23/2009	0.2	14.2	0.1	0.002	0.04
		int	5/24/2009	1.1	8.8	0.1	0.001	0.01
	Downslope	c	7/13/2008	5.1	21.2	5.4	0.003	0.12
		c	7/18/2008	12.5	7.3	5.6	0.047	0.05
		c	9/09/2008	10.1	8	1.3	0.01	0.01
		c	4/11/2009	0.3	0.3	0.3	0.002	0.11
		int	7/18/2008	12.5	6.5	7.9	0.053	0.07
		int	9/09/2008	10.1	8.7	1	0.008	0.01
		int	5/23/2009	6.4	13.3	0.7	0.005	0.01

[a]P_E is total event rainfall, T_{LP} is time lag to peak, Q_T is total runoff, Q_P is peak runoff, and Q/P is the runoff ratio. Canopy data are shown with a c and intercanopy data with int.

threshold pattern also appears between these variables. For $P_E \leq 3$ mm, SFS Q_P yield values of ≤ 0.01 Ls^{-1}, while for $P_E \geq 3$ mm, there is an increasing trend of Q_P with a wide range of values (0.01–0.12 Ls^{-1}). Interestingly, NFS Q_P follows a clear positive increase with P_E. Although the data show a threshold-like response of Q_P and T_{LP} to P_E at both, SFS and NFS plots, clearly there are significant differences in the P_E threshold values between the slopes, with higher rainfall amounts needed to produce significant Q on the NFS as compared to the SFS.

Table 3. Characteristics of Recorded Runoff Events on the SFS During the Study Period[a]

	Plot Type		Date (mm/dd/yyyy)	P_E (mm)	T_{LP} (min)	Q_T (L)	Q_P (L/s)	Q/P
SFS	Upslope	c	7/18/2008	15.4	7.7	21.4	0.117	0.16
		c	7/22/2008	8.7	32	2.9	0.004	0.04
		c	8/05/2008	4.1	0.3	16.6	0.026	0.47
		c	8/16/2008	7.4	12.3	1.3	0.006	0.02
		c	8/29/2008	3.8	32.2	1.4	0.009	0.04
		c	9/09/2008	10.3	8.2	25.9	0.082	0.29
		c	4/11/2009	1.7	51.2	0.1	0.002	0
		c	5/23/2009	6.5	52.2	4.4	0.006	0.08
		c	5/23/2009	6.3	11.3	27.2	0.035	0.5
		c	7/31/2009	3.8	59.5	15.5	0.061	0.47
		c	6/08/2009	11	6.8	11.3	0.045	0.12
		int	7/18/2008	15.4	7.5	8.5	0.034	0.06
		int	8/16/2008	7.4	3.2	11.2	0.01	0.17
		int	9/09/2008	10.3	8.2	28.6	0.093	0.32
		int	4/11/2009	1.7	51.2	1.1	0.003	0.07
		int	5/22/2009	3.4	40.2	3.9	0.003	0.13
		int	5/23/2009	6.5	51.8	0.2	0.002	0
		int	5/23/2009	6.3	12.3	79	0.072	1.44
		int	5/24/2009	1.4	4.2	8.8	0.004	0.72
		int	7/31/2009	11	7.3	10	0.038	0.1
	Downslope	c	7/18/2008	15.4	7.7	13.6	0.114	0.1
		c	8/16/2008	7.4	12.8	1.7	0.012	0.03
		c	9/09/2008	10.3	8.2	15.5	0.053	0.17
		c	4/11/2009	1.7	51.5	0.2	0.005	0.02
		c	5/23/2009	6.5	53.5	0.5	0.004	0.01
		c	5/23/2009	6.3	11.5	0.5	0.004	0.01
		c	7/31/2009	3.8	59	5.1	0.036	0.15
		c	6/08/2009	11	7.2	9	0.036	0.09
		c	9/18/2009	4.4	15.7	2.5	0.008	0.07
		int	7/18/2008	15.4	7.5	7.4	0.073	0.06
		int	9/09/2008	10.3	8.2	5	0.019	0.06
		int	4/11/2009	1.7	51.5	0.1	0.003	0.01
		int	5/23/2009	6.3	11.3	25.5	0.034	0.47
		int	7/31/2009	3.8	1	2.7	0.012	0.08
		int	6/08/2009	11	7.2	5.2	0.022	0.05

[a]P_E is total event rainfall, T_{LP} is time lag to peak, Q_T is total runoff, Q_P is peak runoff, and Q/P is the runoff ratio. Canopy data are shown with a c and intercanopy data with int.

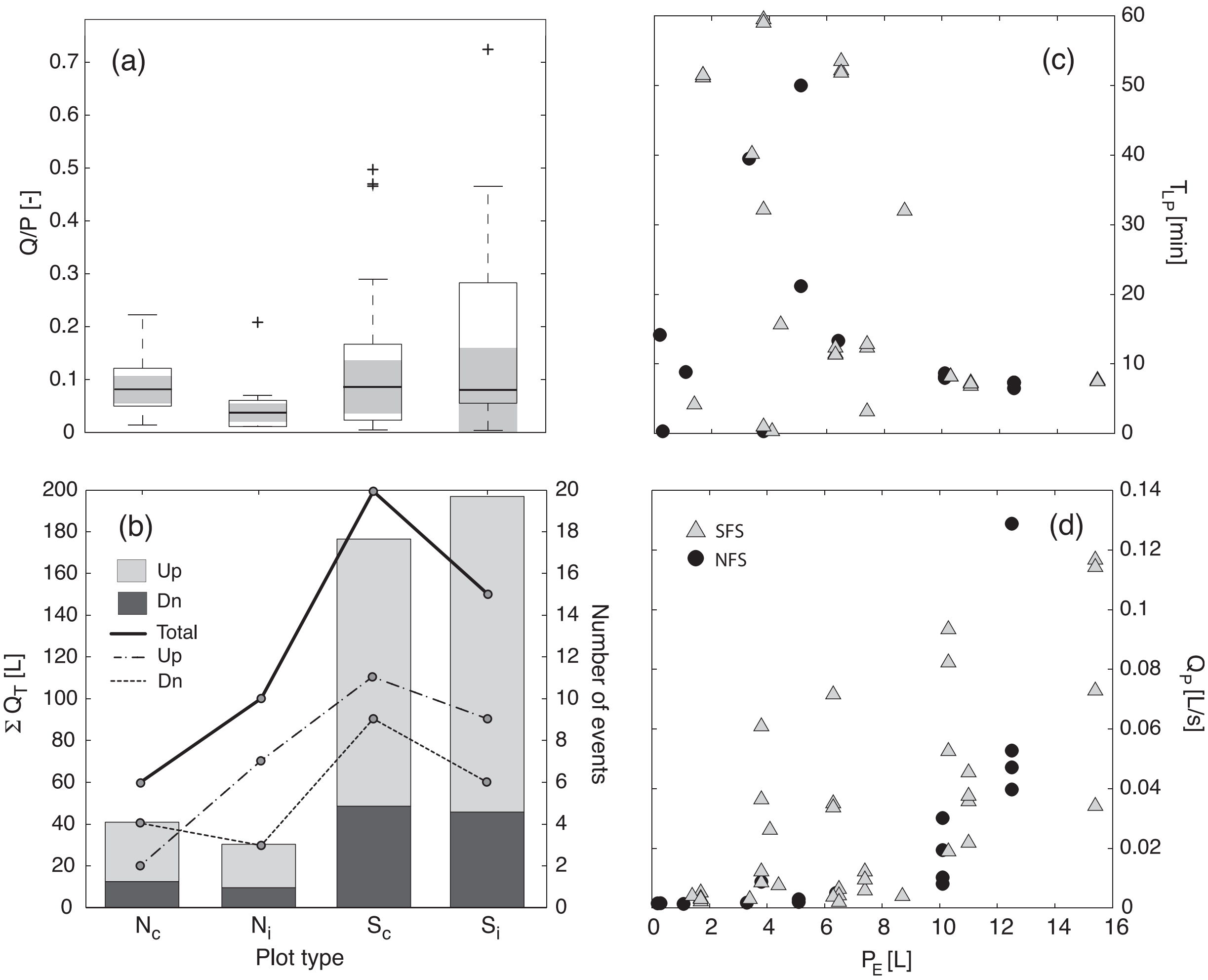

Figure 10. (a) Boxplots of event runoff ratio for each plot type: north facing canopy (N_c), north facing intercanopy (N_i), south facing canopy (S_c), and south facing intercanopy (S_i); (b) bar plots of total runoff for each plot type, N_c, N_i, S_c, and S_i. Each bar is divided by contribution of upslope (light gray) and downslope (gray) locations. The lines depict the number of events producing runoff for the downslope (dotted), upslope (dashed), and the total (solid) for each plot type. Scatterplots of (c) time lag to peak (T_{LP}), and (d) peak runoff (Q_P) as a function of total event rainfall (P_E).

3.5. Energy Fluxes and Evapotranspiration of the Opposing Slopes

[32] The quantification of evapotranspiration (ET) and the differences in energy fluxes in the opposing ecosystems is central to this study. Figure 11 shows time series of rainfall at the Control (a), ET (b) and midday evaporative fraction (EF) at each location (c), and the differences in midday available energy ($\Delta(R_n - G)$; (d) and daily sensible heat flux (ΔH) between the opposing NFS and SFS and the Control (e). Careful inspection reveals that ET in the NFS (ET_{NFS}) is always lower than ET at Control ($ET_{Control}$) and SFS (ET_{SFS}), except for a short period between April and May 2009. While ET_{SFS} and $ET_{Control}$ are similar for the most part, there are slight differences during the summer and portions of the fall and winter seasons. From late spring to late summer, the responses of $ET_{Control}$ to significant ($\geq$5 mm) rainfall pulses are stronger than those of ET_{SFS}, possibly a result from higher wind speeds at the Control. In contrasts, slightly larger ET_{SFS} as compared to $ET_{Control}$ is observed during the fall and winter months, reflecting the larger SFS available energy ($R_n - G$). Because ($R_n - G$) is always larger on SFS, the evaporative fraction (EF_{SFS}) is lower than EF_{NFS} and $EF_{Control}$ throughout the year. The modulating effect of topography on the energy fluxes leading to different ET rates in the opposing slopes is clearly shown by the differences in available energy ($\Delta(R_n - G)$) and sensible heat flux (ΔH) between the NFS and SFS and the Control. Differences in both midday ($R_n - G$) and H reach a minimum ($\leq$2 MJ) during late spring through early summer and peak ($\geq$6 MJ) during late fall and early winter. The differences in ET between NFS and SFS, and between Control and SFS are nevertheless larger in the early fall, specifically during the month of October, when there is still available moisture from the last rainfalls of the summer season and an increasing difference in ($R_n - G$). Finally, because the differences in H mimic those of ($R_n - G$), under similar moisture conditions, the differences in ET between the slopes may be proportional to the differences

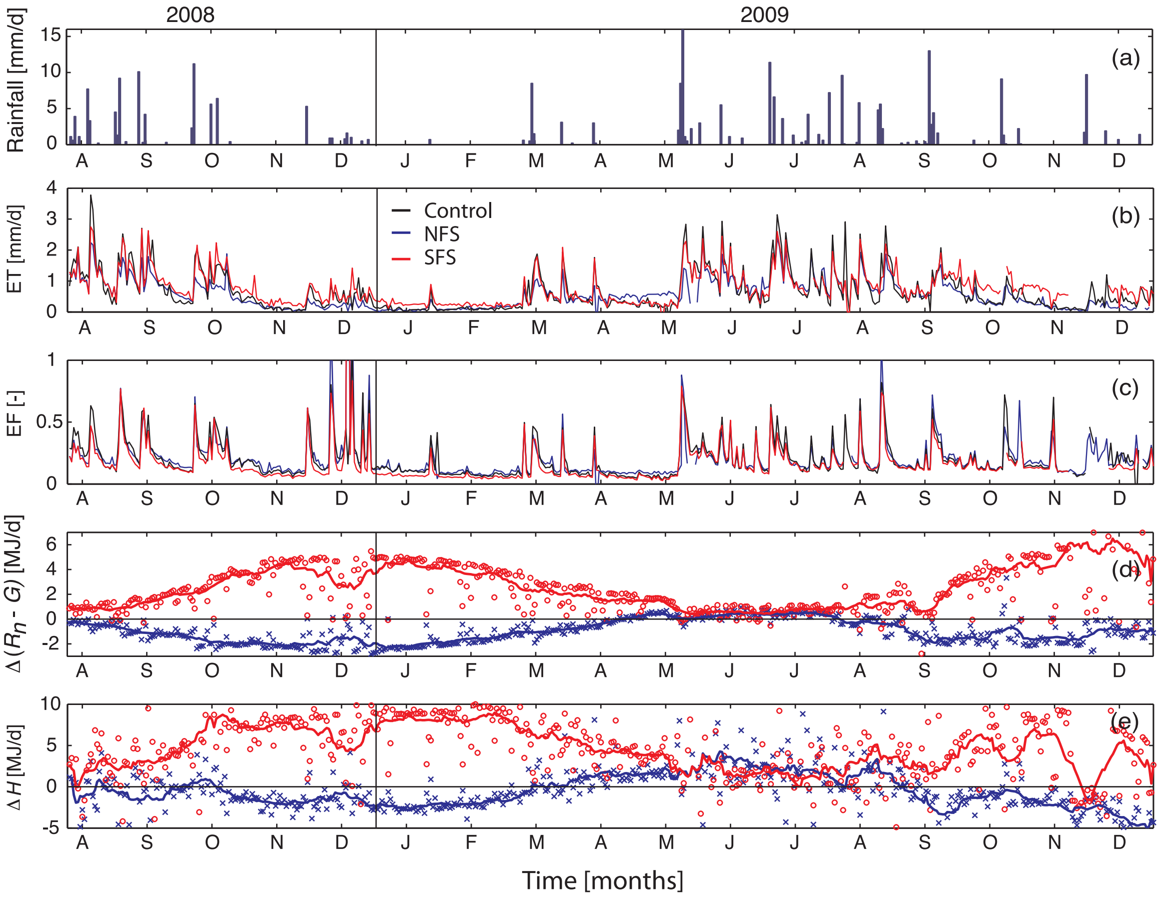

Figure 11. Time series of: (a) rainfall at the Control; (b) evapotranspiration (ET); (c) midday evaporative fraction (EF); differences in midday available energy ($\Delta(R_n - G)$) with the Control for the NFS (blue) and SFS (red), and; differences in total daily sensible heat (ΔH) with the Control for the NFS (blue) and SFS (red) locations.

in ($R_n - G$). This observation supports the argument of a strong topographic regulation of ET dynamics in the opposing slopes via the modulation of the available energy ($R_n - G$) in the catchment.

3.6. Water Balance Partitioning of the Opposing Slopes

[33] An analysis of the evapotranspiration and soil moisture relations in the opposing slopes can reveal insights into the water balance partitioning and the sources of ET for the different ecosystems. For this purpose, we calculated the amount of water removed from the soil by determining the cumulative negative change in moisture ($\Delta\theta$) integrated at each monitoring depth (Z_r) and for each season ($\Delta\theta * Z_r = \Delta\theta_{Zr}$). Figure 12a shows the fraction of ET contributed by soil moisture from each sampling depth (i.e., 10 and 20 cm) against the total ET for each season. Two observations stand out. First, seasonal ET and $\Delta\theta_{Zr}$/ET follow a sinusoidal pattern on both slopes with $\Delta\theta_{Zr}$/ET exhibiting a dampening with soil depth. Second, the seasonal pattern of $\Delta\theta_{Zr}$/ET is in phase with the seasonal ET in the south facing slope, while $\Delta\theta_{Zr}$/ET is out of phase with ET in the north facing slope. The opposite behavior of $\Delta\theta_{Zr}$/ET in the NFS and SFS is an indication of distinct soil water pools for ET for each slope. During the summer, the majority of ET in the NFS is obtained from shallow soil layers (i.e., 0–7 cm) (Figure 12). As time progress, a larger proportion of the ET demand in the NFS is supplied by the deeper soil moisture pool. On the other hand, the contribution of the shallow soil moisture to ET in SFS seems to follow the rainfall seasonality, contributing a larger proportion of ET when there is more rainfall [*Boulanger*, 2004]. Despite the small fraction of total ET (>19% in the NFS and >10% in the SFS) that is explained by moisture depletion at 10 and 20 cm depth in both slopes, the differences in the dynamics of ET-soil moisture relations between the opposing ecosystems revealed by this analysis are unequivocal. Nevertheless, we note that the magnitude of the $\Delta\theta_{Zr}$/ET values might be underestimated by an overestimation of the ET term as obtained by the BREB technique. A number of studies have shown that it is possible for the BREB to yield larger than actual ET estimates in water limited environments [*Barr et al.*, 1994; *Dugas et al.*, 1991] due to a combination of factors, such as: an occasionally unmet assumption of equal diffusivities of water vapor and heat and/or inadequate energy balance estimates due to an insufficient fetch for an equilibrium boundary layer [*Ohmura*, 1982]. Hence, the actual total ET values might be ~10–20% lower than shown in this study. However, given that the inherent limitations of the BREB

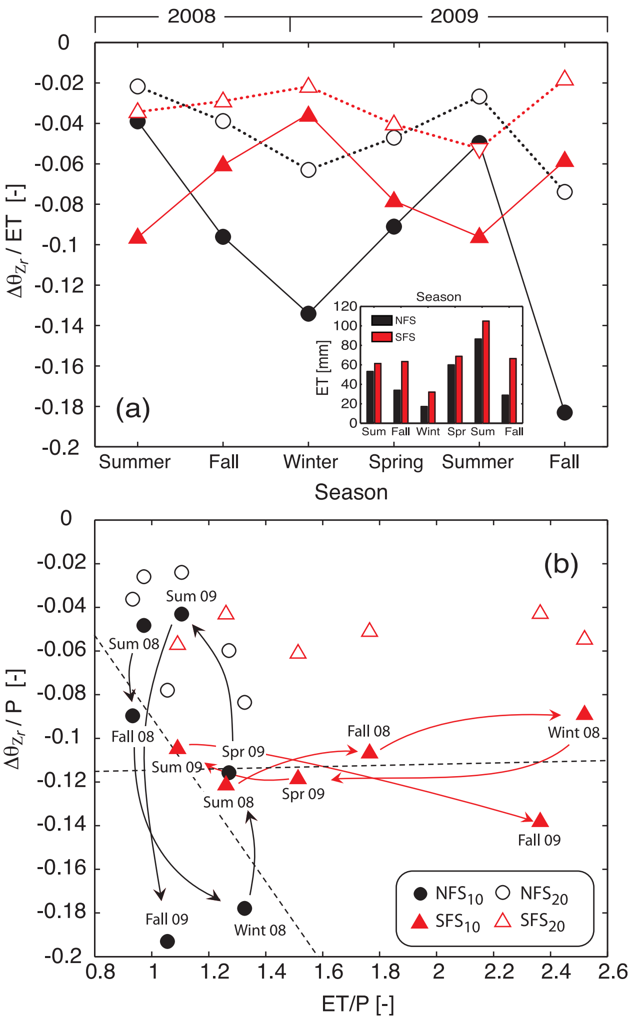

Figure 12. (a) Average fractional contribution of soil moisture to ET ($\Delta\theta_{Zr}$/ET) for each season, slope, and depth. Inset plot shows the total ET for each season. (b) Seasonal climograph of the mean $\Delta\theta_{Zr}$/P as a function of ET/P. For reference, the dashed lines show the linear regressions for NFS_{10} (diagonal) and SFS_{10} (horizontal) data, and the arrows depict the seasonal trajectories of $\Delta\theta_{Zr}$/P versus ET/P.

technique for ET calculations occur in both ecosystems, we believe that the dynamics of the fluxes and the relative differences in water balances between the slopes are valid.

[34] To further explore the observed relations between ET and soil moisture, we constructed a climograph for the NFS and SFS (Figure 12b) in a similar way to *Mahmood and Vivoni* [2011]. In this study, $\Delta\theta_{Zr}$/P is the amount of soil water removed from a particular depth and ET/P is the seasonal evapotranspiration, both as a fraction of the seasonal rainfall. We utilize arrows connecting the climograph points to depict the seasonal trajectories of the water balance on the opposing slopes at the 10 cm depths. Note distinct seasonal trajectories on the water balance of the opposing slopes that is more variable at 10 cm. On the NFS, the summer and fall rainfall events supply sufficient water for ET demands (ET/P $\approx$ 1), while winter and spring precipitation do not suffice, in such a way that stored water from prior seasons might be used (ET/P > 1). On the other hand, on the SFS only the summer rainfalls seem to meet the ET demands (ET/P $\approx$ 1), while the remainder of the year has ET that far exceeds precipitation (ET/P $\gg$ 1), indicating the greater use of deeper stored soil moisture. On the SFS, ET/P varies greatly with the season ($1 < ET/P_{SFS} < 2.5$), with fall and winter ET exceeding P greatly, while $\Delta\theta_{Zr}$/P remains relatively constant at both depths. The combination of a wide range of ET/P >1 and a narrow range on $\Delta\theta_{Zr}$/P for the SFS indicates that the fraction of rainfall water contributed by θ to ET at both depths is always the same, and for that reason the extra water should come from deeper soil layers. On the other hand, the variation of ET/P on the NFS is remarkably smaller ($0.95 < ET/P_{NFS} < 1.33$) than on its SFS counterpart, but the variation in $\Delta\theta_{Zr}$/P is notably larger at both depths. This indicates that NFS uses considerably less deep storage of soil water to meet ET demand and that a greater fraction is from shallow soil layers. This analysis suggests that ET on the NFS is mainly supported by shallow soil moisture, while the SFS contains shrubs that use deep moisture sources within the caliche horizon (i.e., >2 m depth) when shallow layers are dry. While this is feasible for the creosote shrubs and their ability to extract water from deep and highly indurated $CaCO_3$ horizons [*Duniway et al.*, 2010], this will require sufficient moisture reaching those depths from preferential pathways (e.g., root macropores or calcium carbonate dissolution cracks), possibly during large rainfall events. Additionally, the large imbalances shown in the drier seasons maybe exaggerated by the overestimation of ET resulting from the limitations of the BREB technique employed and discussed earlier.

4. Discussion

4.1. Topographically Modulated Energy Balance and Microclimatic Conditions

[35] In the study basin, the energy fluxes of the opposing slopes are primarily controlled by the topographic modulation of the radiation balance, of which the major component is SW_{in}. Comparisons of SW_{in} in the two slopes are in agreement with estimates from spatial radiation modeling by *Gutiérrez-Jurado and Vivoni* [2013b] in the study basin and with other studies simulating near ground SW_{in} in synthetic slopes of north and south aspects [*Zou et al.*, 2007]. More importantly, the radiation balance directly impacts evapotranspiration by altering the available energy for latent heat transfers on each slope. Specifically, the NFS receives 8 MJ less available energy in the fall and winter at midday, and nearly 2 MJ of lower available energy fluxes at midday in the spring and summer seasons as compared to the SFS. Comparisons to midday available energy of a grassland and shrubland from a nearby area yielded similar values for the growing season (i.e., June–September) [*Kurc and Small*, 2004].

[36] Local conditions such as soil moisture and vegetation type comprise second-order controls on the energy balance through their effects on albedo and soil heat fluxes [*Kurc and Small*, 2004]. In the study catchment, albedo on the NFS increases considerably during the late fall and winter, coinciding with the time of minimum incoming radiation, while the albedo on the SFS remains relatively high

and constant throughout the year. On the other hand, G on the NFS remains relatively low for all seasons, in part due to the effect of the tree canopies in effectively reducing the amount of radiation reaching the ground [*Zou et al.*, 2007]. On the NFS, canopy cover also interacts with topographic slope and aspect to amplify energy balance differences as shown by *Gutiérrez-Jurado and Vivoni* [2013b]. The further modulation of the energy balance by the canopies of the juniper trees imprints a spatial heterogeneity in the microclimate of the NFS ecosystem [*Breshears et al.*, 1997], creating a mosaic of low soil temperature patches throughout the slope. This is illustrated by the significant differences in soil temperatures between canopy and inter canopy locations and their remarkable distinct moisture recessions times (Figures 6c, 8, and 9). This intraslope microclimatic heterogeneity of the NFS is not observed in its SFS counterpart. Furthermore, we verified that differences in radiation fluxes between the opposing slopes translated into distinct magnitudes of other microclimatic variables. For example, we recorded larger vapor pressure deficits ($\sim$10% on average) on the SFS as compared to the NFS during the winter and spring seasons. Similarly, we found large differences in T_s ($\sim$10°C) and moderate variability in T_a ($\sim$0.5°C) between the opposing slopes during the periods with largest available energy divergences. Additionally, these microclimatic differences were found to be in phase with the topographic modulation of energy fluxes in the catchment. These findings are in agreement with those from *Desta et al*. [2004], who reported large differences in microclimate among aspects of the four cardinal directions in a North American watershed of the Appalachians, including significant air temperature differences between mesic (north and east aspects) and xeric (west and southwest aspects) sites. Ultimately, the observed differences in microclimatic properties can have important ecological and plant succession implications on the coexisting ecosystems [*Breshears et al.*, 1998; *Chen et al.*, 1999]. For example, microclimatic properties such as soil temperature have been shown to provide a feedback mechanism inducing the encroachment of shrubs into grasslands in the northern Chihuahuan Desert [*D'Odorico et al.*, 2010].

4.2. Topographic-Vegetation Controls on Soil Moisture Dynamics

[37] In a study on the Mackenzie flats close to our site, *Kurc and Small* [2004] found shallow soil moisture residence times that compared well with time scales (i.e., time constants) for evapotranspiration reductions in a grassland and a shrubland during the summer. In contrast, a poor correlation was observed between ET and the depletion of deeper soil moisture, suggesting the two ecosystems sourced summer ET from shallow soil layers. On the two opposing slopes, our analysis revealed soil moisture recession constants (τ) that seem plausible as compared to τ of 2.5 days (shrub) and 2.8 days (grass) in *Kurc and Small* [2004], with summer τ of 3–4 days on the SFS and 4–5 days on the NFS. During the fall and spring seasons, differences in energy balance and microclimate between the opposing slopes are very similar. However, the τ values for the slopes differ significantly between the two seasons (e.g., by 2–4 days depending on position within the slope), suggesting other factors intervene in defining the rates of soil moisture removal. We hypothesize that the fall season retains a vegetative memory from summer greening of herbaceous and woody plant cover that maintains similar soil moisture depletions on both slopes [*Yoder and Nowak*, 1999; *Castellanos-Pérez et al*., 2008; *Notaro et al*., 2010]. In contrast, the spring season is characterized by mostly evergreen plant transpiration [*Oechel et al*., 1972; *Smith et al*., 1997; *Schott and Pieper*, 1985] due to the slow resurgence of annuals (i.e., grasses and other shrubs) from winter dormancy [*Notaro et al*., 2010]. As a result, the differences between fall and spring season τ illustrate the active role of vegetation on mediating the control of the energy inputs on the rate of soil water extraction, suggesting a legacy or prior effect on soil moisture dynamics by the phenological properties (i.e., plant activity cycles) of the opposing ecosystems. Ecologically, the consistently higher and more permanent soil moisture of the shallow layers on the NFS benefits the more mesic vegetation on that slope.

4.3. Terrain-Ecosystem Impacts on Water Balance Partitioning

[38] Since the opposing NFS and SFS ecosystems have similar rainfall inputs, observed differences in runoff (Q) and evapotranspiration are a result of local slope attributes in terms of energy balance, microclimate, and land surface conditions (e.g., vegetative cover, slope degree, soil development). Although Q comprises only a small percent (<7% in the SFS and <0.1% in the NFS) of the total water inputs, the large differences in the runoff frequency and magnitude support the hypothesis of distinct infiltration capacities for each ecosystem [*Gutiérrez-Jurado et al*., 2006], and agrees with the differential runoff responses to large rainfall events documented by *Gutiérrez-Jurado et al*. [2007]. Hydrograph analyses confirm the existence of distinct rainfall-runoff dynamics between the NFS and SFS, including a smaller rainfall threshold ($P_E < 4$ L) to induce a significant runoff response ($Q_p > 0.02 \mathrm{Ls}^{-1}$) in the SFS, as compared to the NFS ($P_E > 10$ L). The variable rainfall-runoff dynamics of each slope reflect distinct erosion capacities and suggest differential sediments and nutrients mobility that can have important implications on the ecology of the opposing ecosystems [*Turnbull et al*., 2010a, 2010b]. Differences in Q thresholds and dynamics are also reflected in the terrain properties shown previously [*Yetemen et al*., 2010]. For example, the larger and more frequent runoff in the SFS can be related directly to the more active erosional features that are evident in the field [*Gutiérrez-Jurado et al*., 2007] and can be identified in terrain analyses with moderate [*Istanbulluoglu et al*., 2008] and high resolution topographic data [*Gutiérrez-Jurado and Vivoni*, 2013a].

[39] Evapotranspiration dynamics are highly influenced by the energy loads on each opposing slope. Since the energy balance of the slopes are seasonally modulated by the effect of aspect on the incoming irradiance, the magnitudes and responses of ET to rainfall inputs vary greatly with the season. Additionally, because both ecosystems have ET demands that typically exceed the availability of water, the evaporative fractions on each slope are similar. Nevertheless, discernible differences in both EF and ET occur right after significant rainfall pulses when differences

in available energy ($R_n - G$) are larger (in the fall and winter). As a result, over the entire study period, the cumulative ET was 38% higher in the SFS than in the NFS. We suggest that the significantly larger cumulative ET on the SFS is due to sustained higher evaporative demands and the recognized ability of the creosote shrubs to extract water from deep and dry soil [*Gibbens*, 2001; *Duniway et al.*, 2010; *Castellanos-Pérez et al.*, 2008]. This can be discerned in the modification of micrometereorological variables which have a cumulative effect on total evapotranspiration. For example, the VPD at the SFS is 8–10% larger than in the NFS and coincides with sustained high incoming radiation values during the winter months. In addition, soil temperatures during the winter are as much as 10°C higher in the SFS as compared to the NFS, and wind speeds are 30% higher in the SFS. As a result, the effective conditions for soil moisture removal by ET are more constant throughout the year in the SFS as compared to the NFS or the Control. This has a direct impact in the water balance of the opposing slopes that varies substantially with the season. For example, it is clear that water deficits are more frequent and extreme on the SFS, reflecting large and sustained ET demands throughout the year, while the NFS maintains a more steady balance between water inputs and outputs especially during the summer and fall. It is also worth noting that the larger soil moisture storage and retention capacities on the NFS and lower ET demands help maintain significantly lower water deficits as compared to the SFS.

[40] Contrasting the coupled effects of terrain aspect, vegetation cover, and soil conditions on the dynamics of water fluxes and balances is a first step toward a better understanding of landscape dynamics on complex terrain. In this study, the NFS and SFS represent two extremes on a spectrum of terrain orientations, where the development of microclimatic differences results in the establishment of dissimilar vegetation types, soil conditions, and hydrologic regimes. We hypothesize that variations in aspect and slope (i.e., inclination) in water-limited regions reduce or enhance the seasonal amplification of microclimatic variables such as temperature and humidity, with direct impacts on soil moisture residence times. Ultimately, these variations in aspect and slope could alleviate or aggravate the effect of extreme and/or prolonged water deficits and temperatures that could trigger vegetation mortality and the associated vegetation cover changes in semiarid ecosystems [*Allen and Breshears*, 1998]. Field and modeling studies using gradient analyses [*Breshears et al.*, 2008; *Kelly and Goulden*, 2008] in aspect-delimited hillslopes with similar vegetation types but varying vegetation cover should provide insights into the susceptibility of arid and semiarid ecosystems to predicted changes in climatic patterns [*Intergovernmental Panel on Climate Change (IPCC)*, 2007].

5. Concluding Remarks

[41] In this study, we investigated the differential dynamics of energy and water fluxes of a semiarid catchment with swift transitions in vegetation types and cover following changes in terrain aspect. By means of an extensive network of sensors, we quantified the differences in energy balance, evapotranspiration, runoff, soil moisture, and micrometeorology in each ecosystem. We found that topographically modulated radiation on the opposing slopes impacts directly the dynamics of evapotranspiration leading to distinct soil moisture residence times, while vegetation becomes a second-order control at the onset of the growing season. The overall result is reflected in the contrasting trajectories of the seasonal water balances of the NFS and SFS throughout the year. The differential ET rates for slopes with contrasting north and south aspects were identified as due to the cumulative effects of differences in incident radiation, consistent with *Segal et al.* [1985]. Throughout this work, we found direct evidence of the differences in the micrometeorology, energy, and water fluxes induced by aspect variations and their coevolved soil and vegetation conditions. Furthermore, this study clearly illustrates that the NFS and SFS use distinct soil water pools for evapotranspiration, have different rainfall-runoff regimes, and preserve remarkably distinct soil moisture conditions year round. On the NFS, we found that ET is largely supported by shallow soil moisture, while in the SFS, the shallow moisture is rapidly depleted and a larger portion of the water for ET should be coming from deeper soil moisture by means of shrub transpiration. Our findings show that the combination of vegetation and terrain characteristics lead to unique hydrologic dynamics on each slope sustaining the necessary contrasts in moisture conditions that maintain the observed ecosystem patterns. The results of this study have important implications for the understanding of the potential causes and effects of vegetation changes in semiarid areas with sloping terrains under variable climatic forcing. Additionally, this study provides both a conceptual framework for the systematic study of different vegetation-terrain-hydrologic interactions in other locations and a valuable data set for the parameterization and validation of ecohydrological modeling efforts.

Appendix A: Correction for Horizontally Based Radiation Measurements on Sloped Terrain

[42] According to *Tian et al.* [2001], the SW_{in} of a sloping surface can be calculated from

$$SW_{in} = Q_r + D_r + A_r, \tag{A1}$$

where Q_r is the irradiance received by the surface directly from the solar beam, D_r is the amount of diffuse radiation reaching the ground and emitted isotropically from all sky directions, and A_r is the radiation received on the surface by reflection from blocking terrain. The terms in equation (A1) are calculated as

$$Q_r = G_m \cdot R_d \cdot (1 - K_r), \tag{A2}$$

$$D_r = G_m \cdot f_\beta \cdot K_r, \tag{A3}$$

$$A_r = G_m \cdot alb \cdot (1 - f_\beta), \tag{A4}$$

where G_m is the global incoming radiation measured on a horizontal surface and R_d is the ratio of direct radiation on the slope (K_{ETsl}) to direct radiation on a horizontal surface (K_{ETh}):

$$R_d = \frac{K_{ETsl}}{K_{ETh}}. \quad \text{(A5)}$$

[43] A detailed derivation of the terms in equation (A5) is described in subsections A1. and A2.. K_r is the ratio of diffuse to global radiation; f_β is a slope reduction factor accounting for the portion of the sky hemisphere above the slope surface that is blocked by the horizontal plane [*Tian et al*., 2001]; and *alb* is the albedo obtained as $alb = SW_{in}/SW_{out}$. The ratio of diffuse to global radiation can be obtained as

$$K_r = a \cdot K_t + b = f \cdot \frac{G_h}{H_o}, \quad \text{(A6)}$$

where K_t is the ratio of global (G_h) to extraterrestrial radiation (H_0) and a and b are empirical coefficients related to local climatic conditions. The slope reduction factor f_β is obtained by

$$f_\beta = 1 - \frac{\beta}{180}, \quad \text{(A7)}$$

where β is the slope angle of the terrain in degrees.

A1. Calculation of the Instantaneous Direct Radiation on a Horizontal Surface

[44] The instantaneous direct radiation on a horizontal plane K_{ETh} is calculated following Iqbal (1983) as

$$K_{ETh} = I_{sc} \cdot E_o[(\cos(\delta) \cdot \cos(\Lambda) \cdot \cos(\omega \cdot t_d) + \sin(\delta) + \sin(\Lambda)], \quad \text{(A8)}$$

where $I_{sc} = 1367$ W m^{-2} is the average radiation flux on a plane perpendicular to the solar beam in the upper atmosphere; E_0 is an eccentricity correction factor that accounts for changes in the relative distance between the Sun and the Earth, calculated daily as

$$E_o = \left(\frac{r_o}{r}\right)^2 = 1.00011 + 0.034221 \cdot \cos(\Gamma) + 0.00128 \cdot \sin(\Gamma) + 0.000719 \cdot \cos(2 \cdot \Gamma) + 0.000077 \cdot \sin(2 \cdot \Gamma), \quad \text{(A9)}$$

where r_0 is the average Sun-Earth distance (km), r is the actual Sun-Earth distance (km), and Γ is day angle (degrees) calculated as

$$\Gamma = \frac{2 \cdot \pi \cdot (J-1)}{365}, \quad \text{(A10)}$$

where J is the Julian day of the year; δ is the declination angle (degrees) that incorporates the effect of the angle between a horizontal plane on the Earth and the solar beam and is computed as

$$\delta = \left(\frac{180}{\pi}\right) \cdot [0.006918 - 0.399912 \cdot \cos(\Gamma) + 0.070257 \cdot \sin(\Gamma) - 0.006758 \cdot \cos(2 \cdot \Gamma) + 0.000907 \cdot \sin(2 \cdot \Gamma) - 0.002697 \cdot \cos(3 \cdot \Gamma) + 0.000148 \cdot \sin(3 \cdot \Gamma)]. \quad \text{(A11)}$$

[45] Λ is latitude (degrees); ω is the angular velocity of the Earth's rotation (15 hr^{-1}); and t_d is the time before or after the solar noon (S_h) in hours and is calculated as a piecewise function:

$$t_d = \begin{cases} S_h - t & \text{if } t < S_h \\ S_h + t & \text{if } t > S_h, \end{cases} \quad \text{(A12)}$$

with S_h computed as

$$S_h = 12 - \left(\frac{E_{rc}}{60}\right) - \left(\frac{105 - \Omega}{15}\right), \quad \text{(A13)}$$

where Ω is the longitude of the plane and E_{rc} is the equation of time in hours, obtained as

$$E_{rc} = 987 \cdot \sin(2 \cdot \beta_{rc}) - 7.53 \cdot \cos(\beta_{rc}) - \cos(\beta_{rc}) - 1.5 \cdot \sin(\beta_{rc}), \quad \text{(A14)}$$

where β_{rc} is a day time adjustment calculated for each day (J) as

$$\beta_{rc} = \frac{360 \cdot (J - 81)}{364}. \quad \text{(A15)}$$

A2. Calculation of the Instantaneous Direct Radiation on a Sloping Surface

[46] The instantaneous direct radiation on a sloping plane K_{ETsl} follows [*Dingman*, 2000], based on the concept of the equivalent slope by *Lee* [1964]. The method is based on the fact that the solar beam angle of incidence on a sloping plane at a given geographic location is equivalent to the angle of incidence on a horizontal plane at a different location with as many degrees removed or added to the original site coordinates. The method as outlined by *Dingman* [2000] was modified to obtain instantaneous rather than daily values.

[47] K_{ETsl} is calculated by

$$K_{ETsl} = I_{sc} \cdot E_o \cdot [(\cos(\delta) \cdot \cos(\Lambda_{eq}) \cdot \cos(\omega \cdot t_{eq} + \Delta\Omega) + \sin(\delta) + \sin(\Lambda_{eq})], \quad \text{(A16)}$$

where Λ_{eq} is the equivalent latitude of the horizontal plane and is obtained as

$$\Lambda_{eq} = \sin^{-1}[\sin(\beta) \cdot \cos(\alpha) \cdot \cos(\Lambda) + \cos(\beta) + \sin(\Lambda)], \quad \text{(A17)}$$

where α is the slope azimuth or aspect orientation (degrees clockwise from north = 0); $\Delta\Omega$ is the longitude difference between the equivalent plane and the original slope [*Dingman*, 2000], computed as

$$\Delta\Omega = \tan^{-1}\left[\frac{\sin(\beta) \cdot \sin(\alpha)}{\cos(\beta) \cdot \cos(\Lambda) - \sin(\beta) \cdot \sin(\Lambda) \cdot \cos(\alpha)}\right]. \quad \text{(A18)}$$

t_{eq} is the equivalent time before or after the solar noon for the original sloping surface (S_{sl}) and is calculated as a piecewise function

$$t_{eq} = \begin{cases} S_{Sl} - t & \text{if } t < S_{Sl} \\ S_{Sl} + t & \text{if } t > S_{Sl}. \end{cases} \quad \text{(A19)}$$

[48] The value for S_{Sl} is computed by adjusting the solar noon of the original longitude to the time offset (T_{offset}) of $\Delta\Omega$ as

$$S_{Sl} = 12 - \left(\frac{E_{rc}}{60}\right) - \left(\frac{105 - (\Omega + T_{offset})}{15}\right). \quad \text{(A20)}$$

[49] **Acknowledgments.** We would like to thank NASA and NFS for financial support provided through grants NNG05GA17G and EAR0819924, respectively. We also acknowledge the facilities provided by the Sevilleta National Wildlife Refuge. We are grateful to many graduate and undergraduate students that helped on the instrumentation of the study site. We acknowledge the comments from three anonymous reviewers that helped improved this manuscript.

References

Allen, C. D., and D. D. Breshears (1998), Drought-induced shift of a forest-woodland ecotone: Rapid landscape response to climate variation, *Proc. Natl. Acad. Sci. U. S. A.*, *95*(25), 14,839–14,842.

Armesto, J. J., and J. A. Martínez (1978), Relations between vegetation structure and slope aspect in the Mediterranean region of Chile, *J. Ecol.*, *66*(3), 881–889.

Astrom, M., M. Dynesius, K. Hylander, and C. Nilsson (2007), Slope aspect modifies community responses to clear-cutting in boreal forests, *Ecology*, *88*(3), 749–758.

Badano, E. I., L. A. Caviares, M. A. Molina-Montenegro, and C. L. Quiroz (2005), Slope aspect influences plant association patterns in the Mediterranean, *J. Arid Environ.*, *62*, 93–108.

Barr, A. G., K. M. King, T. J. Gillespie, G. D. Hartog, and H. H. Neumann (1994), A comparison of Bowen Ratio and Eddy Correlation Sensible and Latent Heat flux measurements above deciduous forest, *Boundary Layer Meteorol.*, *71*, 21–41.

Bedford, D. (2008), Effects of vegetation-related soil heterogeneity on runoff, infiltration, and redistribution in semi-arid shrubland and grassland landscapes, PhD thesis, pp. 1–197, Univ. of Colorado.

Bedford, D., and E. Small (2008), Spatial patterns of ecohydrologic properties on a hillslope-alluvial fan transect, central New Mexico, *Catena*, *73*(1), 3448, doi:10.1016/j.catena.2007.08.005.

Bennie, J., B. Huntley, A. Wiltshire, M. O. Hill, and R. Baxter (2008a), Slope, aspect and climate: Spatially explicit and implicit models of topographic microclimate in chalk grassland, *Ecol. Modell.*, *216*, 47–59.

Bennie, J., M. O. Hill, R. Baxter, and B. Huntley (2008b), Influence of slope and aspect on long-term vegetation change in British chalk grasslands, *J. Ecol.*, *94*, 355–368.

Bergkamp, G. (1998), A hierarchical view of the interactions of runoff and infiltration with vegetation and microtopography in semiarid shrublands, *Catena*, *33*, 201–299.

Boulanger, J. R. (2004), Stable isotope partitioning of evapotranspiration across a shrub-grass ecotone following a precipitation event Sevilleta National Wildlife Refuge, USA, MS thesis, 66 pp., New Mexico Inst. of Min. and Technol., Socorro, N. M.

Bowen, I. S. (1926), The ratio of heat losses by conduction and by evaporation from any water surface, *Phys. Rev.*, *27*, 779–787.

Brakensiek, D. L., H. B. Osborn, and W. J. Rawls (1979), *Field Manual for Research in Agricultural Hydrology: Agricultural Handbook No. 224*, United States Dep. of Agric., pp. 88–125.

Breshears, D. D., P. M. Rich, F. Barnes, and K. Campbell (1997), Overstory-imposed heterogeneity in solar radiation and soil moisture in a semiarid woodland, *Ecol. Appl.*, *7*(4), 1201–1215.

Breshears, D. D., P. M. Rich, F. J. Barnes, and K. Campbell (1998), Effects of woody plants on microclimate in a semiarid woodland: Soil temperature and evaporation in canopy and intercanopy patches, *Int. J. Plant Sci.*, *159*, 1010–1017.

Breshears, D. D., T. E. Huxman, H. D. Adams, C. B. Zou, and J. E. Davison (2008), Vegetation synchronously leans upslope as climate warms, *Proc. Natl. Acad. Sci. U. S. A.*, *105*(33), 11,591–11,592, doi:10.1073/pnas.0806579105.

Briggs, J. M., A. K. Knapp, J. M. Blair, J. L. Heisler, G. A. Hoch, M. S. Lett, and J. K. McCarron (2005), An ecosystem in transition: Causes and consequences of the conversion of mesic grassland to shrubland, *BioScience*, *55*(3), 243, doi:10.1641/0006–3568(2005)055[0243:AEITCA]2.0.CO;2.

Brooks, P. D., and E. R. Vivoni (2008), Mountain ecohydrology: Quantifying the role of vegetation in the water balance of montane catchments, *Ecohydrology*, *1*(3), 187–192.

Broxton, P. D., P. A. Troch, and S. W. Lyon (2009), On the role of aspect to quantify water transit times in small mountainous catchments, *Water Resour. Res.*, *45*, 115, doi:10.1029/2008WR007438.

Cantlon, J. E. (1953), Vegetation and microclimates on north and south slopes of Cushetunk Mountain, New Jersey, *Ecol. Monogr.*, *23*(3), 241–270.

Castellanos-Pérez, E., A. de Soyza, and G. Donart (2008), Photosynthesis and water use efficiency of the association between Larrea tridentata (DC) Cov. and Muhlenbergia porteri Scribn, *Int. J. Exp. Bot.*, *77*, 297–320.

Chen, J., S. C. Saunders, T. R. Crow, R. J. Naiman, K. D. Brosofske, G. D. Mroz, B. L. Brookshire, and J. F. Franklin (1999), Microclimate in forest ecosystem and landscape ecology, *BioScience*, *49*(4), 288–297.

Chmura, D. (2008), The slope aspect affects the heterogeneity and growth of ground flora vegetation in deciduous temperate forest, *Polish J. Ecol.*, *56*, 463–470.

Coble, D. W., k. s. Milner, and J. D. Marshall (2001), Above- and belowground production of trees and other vegetation on contrasting aspects in western Montana: A case study, *J. For. Ecol. Manage.*, *142*, 231–241.

Cottle, H. J. (1932), Vegetation on north and south slopes of mountains in southwestern Texas, *Ecology*, *13*(2), 121–134.

Desta, F., R. R. Hicks Jr., and J. J. Colbert (2003), Influence of topographic aspect, precipitation and drought on radial growth of four major tree species in an Appalachian watershed, *J. For. Ecol. Manage.*, *177*, 409–425.

Desta, F., J. J. Colbert, J. S. Rentch, and K. W. Gottschalk (2004), Aspect induced differences in vegetation, soil, and microclimatic characteristics of an Appalachian watershed, *Castanea*, *69*(2), 92–108.

Devitt, D. A., and S. D. Smith (2002), Root channel macropores enhance downward movement of water in a Mojave Desert ecosystem, *J. Arid Environ.*, *50*(1), 99108, doi:10.1006/jare.2001.0853.

Dingman, L. S. (2000), *Physical Hydrology*, 365 pp., 2nd ed., Prentice Hall.

D'Odorico, P., J. D. Fuentes, W. T. Pockman, S. L. Collins, Y. He, J. A. Medeiros, S. DeWekker, and M. E. Litvak. (2010), Positive feedback between microclimate and shrub encroachment in the northern Chihuahuan desert, *Ecosphere*, *1*(6), art17, doi:10.1890/ES10–00073.1.

Dugas, W., L. Fritschen, and L. Gay (1991), Bowen ratio, eddy correlation, and portable chamber measurements of sensible and latent heat flux over irrigated spring wheat, *J. Agric. For. Meteorol.*, *56*, 120.

Duniway, M. C., J. E. Herrick, and H. C. Monger (2010), Spatial and temporal variability of plant-available water in calcium carbonate-cemented soils and consequences for arid ecosystem resilience, *Oecologia*, *163*(1), 215–226, doi:10.1007/s00442-009-1530-7.

Fritschen, L. J., and J. R. Simpson (1989), Surface energy and radiation balance systems: General description and improvements, *J. Appl. Meteorol.*, *28*, 680–689.

Gallardo-Cruz, J. A., E. A. Pérez-García, and J. A. Meave (2009), *β*-Diversity and vegetation structure as influenced by slope aspect and altitude in a seasonally dry tropical landscape, *Landscape Ecol.*, *24*(4), 473–482. doi:10.1007/s10980-009-9332-1.

Gibbens, R. (2001), Root systems of some Chihuahuan Desert plants, *J. Arid Environ.*, *49*(2), 221–263, doi:10.1006/jare.2000.0784.

Gutiérrez-Jurado, H. A., E. R. Vivoni, J. B. J. Harrison, and H. Guan (2006), Ecohydrology of root zone water fluxes and soil development in complex semiarid rangelands, *Hydrol. Processes*, *20*, 3289–3316.

Gutiérrez-Jurado, H. A., E. R. Vivoni, E. Istanbulluoglu, and R. L. Bras (2007), Ecohydrological response to a geomorphically significant flood event in a semiarid catchment with contrasting ecosystems, *Geophys. Res. Lett.*, *34*, L24S25, doi:10.1029/2007GL030994.

Gutiérrez-Jurado, H. A., and E. R. Vivoni (2013a), Ecogeomorphic expressions of aspect-controlled semiarid basins: I. Topographic analyses with high resolution datasets, *Ecohydrology*, *6*(1), 8–23, doi:10.1002/eco.280.

Gutiérrez-Jurado, H. A., and E. R. Vivoni (2013b), Ecogeomorphic expressions of aspect-controlled semiarid basins: II. Topographic and vegetation controls on solar irradiance, *Ecohydrology*, *6*(1), 24–37, doi:10.1002/eco.1263.

Gwinn, R. W. (1984), Chute entrances for HS, H, and HL flumes, *J. Hydraul. Eng.*, *110*(5), 587–603, doi:10.1061/(ASCE)0733–9429(1984)110:5(587)).

Gwinn, R. W., and D. A. Parsons (1976), Discharge equations for HS, H, and HL flumes, *J. Hydraul. Div.*, *102*(5), 11,874–11,887.

Holland, P. G., and D. G. Steyn (1975), Vegetational responses to latitudinal variations in slope angle and aspect, *J. Biogeogr.*, *2*, 179–183.

Holland, P. G., D. G. Steyn, and R. F. Fuggle (1977), Habitat occupation by Aloe ferox Mill. (Liliaceae) in relation to topographic variations in direct beam solar radiation income, *J. Biogeogr.*, *4*(1), 61–72.

Huxman, T. E., B. P. Wilcox, D. D. Breshears, R. L. Scott, K. A. Snyder, E. E. Small, K. Hultine, W. T. Pockman, and R. B. Jackson (2005), Ecohydrological implications of woody plant encroachment, *Ecology*, *86*(2), 308–319, doi:10.1890/03–0583.

Intergovernmental Panel on Climate Change (IPCC) (2007), *Climate Change 2007: The Physical Science Basis. Contribution of Working Group I to the Fourth Assessment Report of the IPCC*, Cambridge Univ. Press, Cambridge, U. K.

Istanbulluoglu, E., O. Yetemen, E. R. Vivoni, H. A. Gutiérrez-Jurado, and R. L. Bras (2008), On the topographic imprint of vegetation: Inferences from regional analysis of landscape morphology in central New Mexico, *Geophys. Res. Lett.*, *34*, L14403, doi:10.1029/2008GL034477.

Ivanov, V. Y., R. L. Bras, and E. R. Vivoni (2008a), Vegetation-hydrology dynamics in complex terrain of semiarid areas. I. A mechanistic approach to modeling dynamic feedbacks, *Water Resour. Res.*, *44*, W03429, doi:10.1029/2006WR005588.

Ivanov, V. Y., R. L. Bras, and E. R. Vivoni (2008b), Vegetation-hydrology dynamics in complex terrain of semiarid areas: 2. Energy-water controls of vegetation spatiotemporal dynamics and topographic niches of favorability, *Water Resour. Res.*, *44*, W03430, doi:10.1029/2006WR005595.

Kabat, P., A. J. Dolman, and J. A. Elbers (1997), Evaporation, sensible heat and canopy conductace of a fallow savannah and patterned woodland in the Sahel, *J. Hydrol.*, *188–189*, 494–515.

Kelly, A. E., and M. L. Goulden (2008), Rapid shifts in plant distribution with recent climate change, *Proc. Natl. Acad. Sci. U. S. A.*, *105*(33), 118–236, doi:10.1073/pnas.0802891105.

Kimball, B. A., R. D. Jackson, F. S. Nakayama, S. B. Idso, and R. J. Reginato (1976), Soil-heat flux determination: Temperature gradient method with computed thermal conductivities, *J. Soil Sci. Soc. Am.*, *40*, 25–28.

Knapp, A. K., et al. (2008), Shrub encroachment in North American grasslands: Shifts in growth form dominance rapidly alters control of ecosystem carbon inputs, *Global Change Biol.*, *14*(3), 615–623, doi:10.1111/j.1365–2486.2007.01512.x.

Kurc, S. A., and E. E. Small (2004), Dynamics of evapotranspiration in a semiarid grassland and shrubland ecosystems during the summer-monsoon season, central New Mexico, *Water Resour. Res.*, *40*, W09305, doi:10.1029/2004WR003068.

Kurc, S. A., and E. E. Small (2007), Soil moisture variations and ecosystem-scale fluxes of water and carbon in semiarid grassland and shrubland, *Water Resour. Res.*, *43*, W06416, doi:10.1029/2006WR005011.

Kutiel, P. (1992), Slope aspect effect on soil and vegetation in a Mediterranean ecosystem, *Isr. J. Bot.*, *41*, 243–250.

Kutiel, P., and H. Lavee (1999), Effect of slope aspect on soil and vegetation properties along an aridity transect, *Isr. J. Plant Sci.*, *47*, 169–178.

Lee, R. (1964), Potential insolation as a topoclimatic characteristic of drainage basins, *Bull. Int. Assoc. Sci. Hydrol.*, *9*, 27–41.

Lett, M., and A. Knapp (2004), Influence of shrub encroachment on aboveground net primary productivity and carbon and nitrogen pools in a mesic grassland, *Can. J. Bot.*, *1370*, 1363–1370, doi:10.1139/B04–088.

Liang, E., X. Shao, D. Eckstein, L. Huang, and X. Liu (2006), Topography-and species-dependent growth responses of Sabina przewalskii and Picea crassifolia to climate on the northeast Tibetan Plateau, *For. Ecol. Manage.*, *236*(2–3), 268–277, doi:10.1016/j.foreco.2006.09.016.

Lin, H. (2006), Temporal stability of soil moisture spatial pattern and subsurface preferential flow pathways in the shale hills catchment, *Vadose Zone J.*, *5*, 317–340.

Loik, M. E., D. D. Breshears, W. K. Lauenroth, and J. Belnap (2004), A multi-scale perspective of water pulses in dryland ecosystems: Climatology and ecohydrology of the western USA, *Oecologia*, *141*(2), 269–281, doi:10.1007/s00442-004-1570-y.

Mahmood, T. H., and E. R. Vivoni (2011), A climate-induced threshold in hydrologic response in a semiarid ponderosa pine hillslope, *Water Resour. Res.*, *47*, W09529, doi:10.1029/2011WR010384.

Martínez-Fernández, J., and A. Ceballos (2003), Temporal stability of soil moisture in a large-field experiment in Spain, *J. Soil Sci. Soc. Am.*, *67*, 1647–1656.

Martinez Mesa, E., and W. G. Whitford (1996), Stemflow, throughfall and channelization of stemflow by roots in three Chihuahuan desert shrubs, *J. Arid Environ. 32*, 271–287.

McMahon, D. R. (1998), Soil, landscape and vegetation interactions in a small semiarid drainage basin: Sevilleta National Wildlife Refuge, New Mexico, MS thesis, 174 pp., New Mexico Inst. of Min. and Technol., Socorro, N. M.

Méndez-Barroso, L. A., E. R. Vivoni, C. J. Watts, and J. C. Rodríguez (2009), Seasonal and interannual relations between precipitation, surface soil moisture and vegetation dynamics in the North American monsoon region, *J. Hydrol.*, *377*(1–2), 59–70, doi:10.1016/j.jhydrol.2009.08.009.

Milne, B. T., D. I. Moore, J. L. Betancourt, J. A. Parks, T. W. Swetnam, R. R. Parmenter, and W. T. Pockman (2003), Multidecadal drought cycles in south-central New Mexico: Patterns and consequences, in *Climate Variability and Ecosystem Responses at Long-Term Ecological Research Sites*, edited by D. Greenland, D. G. Goodin, and R. C. Smith, pp. 286–307, Oxford Univ. Press, New York.

Mooney, H. A., E. L. Dunn, F. Shropshire, and L. Song (1975), Vegetation comparisons between the Mediterranean climatic areas of California and Chile, *Flora*, *159*(5), 480–496.

Newman, B. D., B. P. Wilcox, S. R. Archer, D. D. Breshears, C. N. Dahm, C. J. Duffy, N. G. McDowell, F. M. Phillips, B. R. Scanlon, and E. R. Vivoni (2006), Ecohydrology of water-limited environments: A scientific vision, *Water Resour. Res.*, *42*, W06302, doi:10.1029/2005WR004141.

Nie, D., I. E. Flitcroft, and E. T. Kanemasu (1992), Performance of Bowen ratio systems on a slope, *J. Agric. For. Meteorol.*, *59*, 165–181.

Nie, W., Y. Yuan, W. Kepner, C. Erickson, and M. Jackson (2012), Hydrological impacts of mesquite encroachment in the upper San Pedro watershed, *J. Arid Environ.*, *82*, 147–155, doi:10.1016/j.jaridenv.2012.02.008.

Notaro, M., Z. Liu, R. G. Gallimore, J. W. Williams, D. S. Gutzler, and S. Collins (2010), Complex seasonal cycle of ecohydrology in the southwest United States, *J. Geophys. Res.*, *115*, G04034, doi:10.1029/2010JG001382.

Oechel, W. C., B. R. Strain, and W. R. Odening (1972), Tissue water potential, photosynthesis, C-14-labeled photosynthate utilization, and growth in desert shrub Larrea divaricata cav, *Ecol. Monogr.*, *42*, 127–141.

Ohmura, A. (1982), Objective criteria for rejecting data for Bowen Ratio flux calculations, *J. Appl. Meteorol.*, *21*, 595–598.

Parsons, D. J. (1976), Vegetation structure in the Mediterranean scrub communities of California and Chile, *Ecology*, *64*(2), 435–447.

Parsons, D. U., and A. R. Moldenke (1975), Convergence in vegetation structure along analogous climatic gradients in California and Chile, *Ecology*, *56*(4), 950–957.

Pérez, P. J., F. Castellvi, M. Ibanez, and J. I. Rossell (1999), Assessment of reliability of Bowen ratio method for partitioning fluxes, *J. Agric. For. Meteorol.*, *97*, 141–150.

Perkins, S. R., and K. C. McDaniel (2005), Infiltration and sediment rates following Creosotebush control with Tebuthiuron, *Rangeland Ecol. Manage.*, *58*(6), 605–613.

Sandvig, R. C., and F. M. Phillips (2006), Ecohydrological controls on soil moisture fluxes in arid vadose zones, *Water Resour. Res.*, *42 W08422*, doi:10.1029/2005WR004644.

Schott, M. R., and R. D. Pieper (1985), Influence of canopy characteristics of one-seed juniper on understory grasses, *J. Range Manage.*, *38*(4), 328–331.

Schwinning, S., and O. E. Sala (2004), Hierarchy of responses to resource pulses in arid and semi-arid ecosystems, *Oecologia*, *141*(2), 211–220, doi:10.1007/s00442-004-1520-8.

Segal, M., Y. Mahrer, R. A. Pielke, and Y. Ookouchi (1985), Modeling transpiration patterns of vegetation along south and north facing slopes during the subtropical dry Season, *Agric. For. Meterol.*, *36*, 19–28.

Seyfried, M. S., S. Schwinning, M.A. Walvoord, W.T. Pockman, B. D. Newman, R. B. Jackson, and F. M. Phillips (2005), Ecohydrological control of deep drainage in arid and semiarid regions, *Ecology*, *86*(2), 277–287, doi:10.1890/03-0568.

Smith, S. D., R. K. Monsoon, and J. E. Anderson (1997), *Physiological Ecology of North American Desert Plants*, 286 pp., Springer, New York.

Sternberg, M., and M. Shoshany (2001), Influence of slope aspect on Mediterranean woody formations: Comparison of a semiarid and an arid site in Israel, *Ecol. Res.*, *16*, 345–355.

Tian Y. Q., R. J. Davies-Colley, P. Gong, and B. W. Thorrold (2001), Estimating solar radiation on slopes of arbitrary aspect, *J. Agric. For. Meteorol.*, *109*, 67–74.

Tromp-van Meerveld, H. J., and J. J. McDonnell (2006), On the interrelations between topography, soil depth, soil moisture, transpiration rates and species distribution at the hillslope scale, *Adv. Water Res.*, *29*, 293–310.

Turnbull, L., J. Wainwright, and R. E. Brazier (2010b), Nitrogen and phosphorus dynamics during runoff events over a transition from grassland to shrubland in the south-western United States, *Hydrol. Processes*, *25*(1), 1–17, doi:10.1002/hyp.7806.

Turnbull, L., J. Wainwright, and R. E. Brazier (2010c), Changes in hydrology and erosion over a transition from grassland to shrubland, *Hydrol. Processes*, *24*, 393–414, doi:10.1002/hyp.7491.

Turnbull, L., J. Wainwright, R. E. Brazier, and R. Bol (2010a), Biotic and abiotic changes in ecosystem structure over a shrub-encroachment gradient in the southwestern USA, *Ecosystems*, *13*(8), 1239–1255, doi:10.1007/s10021-010-9384-8..

Vivoni, E. R. (2012), Spatial patterns, processes and predictions in ecohydrology: Integrating technologies to meet the challenge, *Ecohydrology*, *5*(3), 235–241.

Vivoni, E. R., C. J. Watts, and J. C. Rodríguez (2010), On the spatiotemporal variability of soil moisture and evapotranspiration in a mountainous basin within the North American Monsoon region, *Water Resour. Res.*, *46*, W02509, doi:10.1029/2009WR008240.

Wang, L., K. K. Caylor, J. C. Villegas, G. A. Barron-Gafford, D. D. Breshears, and T. E. Huxman (2010), Partitioning evapotranspiration across gradients of woody plant cover: Assessment of a stable isotope technique, *Geophys. Res. Lett.*, *37*(9), 17, doi:10.1029/2010GL043228.

Wang, L., S. Wei, R. Horton, and M. Shao (2011), Effects of vegetation and slope aspect on water budget in the hill and gully region of the Loess Plateau of China, *Catena*, *87*, 90–100.

Warren, R. J. (2010), An experimental test of well-described vegetation patterns across slope aspects using woodland herb transplants and manipulated abiotic drivers, *New Phytol.*, *185*(4), 1038–1049, doi:10.1111/j.1469-8137.2009.03147.x.

Whittaker, R. H. (1967), Gradient analysis of vegetation, *Biol. Rev.*, *42*, 207–264.

Yetemen, O., E. Istanbulluoglu, and E. R. Vivoni (2010), The implications of geology, soils and vegetation on landscape morphology: Inferences from semiarid basins with complex vegetation patterns in central New Mexico, *Geomorphology*, *116*, 246–263.

Yoder, C. K., and R. S. Nowak (1999), Soil moisture extraction by evergreen and drought-deciduous shrubs in the Mojave Desert during wet and dry years, *J. Arid Environ.*, *42*(2), 81–96, doi:10.1006/jare.1999.0504.

Zhou, X., E. Istanbulluoglu, and E. R. Vivoni (2013), Modeling the ecohydrological role of aspect-controlled radiation on tree-grass-shrub coexistence in a semiarid climate, *Water Resour. Res.*, *49*, 2872–2895, doi:10.1002/wrcr.20259.

Zou, C. B., G. A. Barron-Gafford, and D. D. Breshears (2007), Effects of topography and woody plant canopy cover on near-ground solar radiation: Relevant energy inputs for ecohydrology and hydropedology, *Geophys. Res. Lett.*, *34*, L24S21, doi:10.1029/2007GL031484.